Deanship of Graduate Studies

Al-Quds University

Asymptotic Models to study the Electromagnetic Scattering from 2D Rough Surface (3D Electromagnetic Problem)

Ashraf Talal Ahmad Rabaia

M.SC. Thesis

Jerusalem - palestine

1439/2018

Asymptotic Models to study the Electromagnetic Scattering from 2D Rough Surface (3D Electromagnetic Problem)

Prepared By:

Ashraf Talal Ahmad Rabaia

B.Sc.: Telecommunication Engineering, Arab American University /palestine

Supervisor: Dr.Mohammad Kouali

A thesis Submitted in Partial Fullfillment of requirements for the degree of Master of Electronic and Computer Engineering, Faculty of Engineering, Al-Quds University

1439/2018

Deanship of Graduation Studies

Al-QUDS University

Electronic and Computer Engineering

Faculty of Engineering

Thesis Approval

Asymptotic Models to study the Electromagnetic Scattering from 2D Rough Surface (3D Electromagnetic Problem

Prepared By : Ashraf Talal Ahmad Rabaia

Registration No.:21420038

Supervisor: Dr.Mohammad Kouali

Master thesis submitted and accepted, Date:19/5/2018

The names and signatures of the examining committee members are as follows:

1- Head of Committee: Dr.Mohammad Kouali Signature .....

2- Internal Examiner: Dr.Yousef Zahaykah Signature .....

2- External lExaminer: Dr.Isam Alawneh Signature Isam Alawneh

Jerusalem - palestine
1439/2018

Declaration

I Certify that this thesis submitted for the degree of master is the result of my own research, except where otherwise acknowledged, and that this thesis (or any part of the same) has not been submitted for a higher degree to any other university or institution.

Signed: .....

Ashraf Talal Ahmad Rabaia

Date: 3-6-2018

Dedication

I dedicate this work to my:

Mother, wife Haya, daughters Jana and Leen, brothers, sister, uncle Dr.Hussin Alaraj, aunts, uncles, friends and all of my family

Acknowledgments

First of all, I would like to thank the Almighty ALLAH whose blessing have always been prevailed on us. My sincere thanks to all people who shared me their feelings, supported and helped me to finish my thesis.

I'm greatly honored and thankful to my supervisor Dr. Mohammed Kouali for his guidance, encouragment, advices and insightful comments throughout the thesis period.

I would like to express my sincere gratitude and appreciation to President Office represented by president Mahmoud Abbas for giving me the opportunity to learn and spread the light of education.

I would like to express my special thanks to the staff of the Faculty of Engineering at AL-Quds University who taught me during my Master degree studies.

Contents

List of Figures

Abstract

The investigation of the problem of wave scattering from interfaces is important for many scientific and engineering disciplines such as photorealistic image generation in computer graphics, the manufacture of the semiconductors. Nowadays, the research in this domain continues, because multiple applications exist such as in telecommunication, medical imagery, military operations, and radar remote sensing. Rigorous methods such as the Method of Moments (MOM) are widely developed to calculate the Radar Cross Section (RCS) [1]. These rigorous models have the advantage of being exact, but they require, in general, a long computation time and a large memory space.

Thus, it is of interest to use asymptotic models such as Kirchhoff Approximation (KA), which have the great advantage of being faster to compute, less complexity and little computational time. Because of their complexity, the rigorous models usually allow us to treat surfaces with restricted dimensions (typically, $30\lambda \times 30\lambda$ for 3D problems) [2]; whereas the asymptotic models usually permit to treat larger surfaces. However, asymptotic models are applicable only in a restricted validity domain. Indeed, the models are used for resolving the problem more easily and/or more rapidly. KA is one of the widely used high-frequency asymptotic techniques to accelerate the radar cross section calculation [4].

The purpose of this work is to adopt a mathematical model using KA to calculate the scattered fields from a random rough surface (sea like surface) for

a 3D electromagnetic problem and make a comparison with rigorous method to validate it, then insert correction factor called shadowing function to the approximation (KA), which depends on roughness parameters and incident angles. A reference method is required to validate the domain of the proposed approaches so, the Multilevel Fast Multi-Pole Method (MLFMM) of Electromagnatic Field (EM) simulator FEKO has been chosen as a reference model for the calculation of rough surface RCS, to determine the validity domain KA approach. The comparison occurs for observation angles between $[-90^\circ : +90^\circ]$.

This work is organized as follows: first, we introduce some concepts and basic principles in electromagnetic theory necessary to introduce our work such as the random rough surface statistical description, incident and reflection from rough surface, integral equation based on Huygens principle and so on. Then a computational methods of rough surface scattering is introduced showing its properties and validity domain.

In chapter two, a mathematical model for 3D rough surface scattering problem is presented using KA, showing its properties and validity domain. Indeed, the radar cross section results obtained from the KA model is compared to rigorous algorithms to validate the method.

Finally in the last chapter, the shadowing function is inserted into KA approximation to improve the technique and take into account the region that affected from the shadowing phenomenon. In addition, the Iterative Physical Optics (IPO) method is discussed in the last section to compared with KA since this technique is based on KA but in an iterative way.

Chapter 1

Electromagnetic Wave Scattering from Random Rough Surface: Basics

---

This work is motivated by numerous applications of microwave remote sensing of perfectly-conducting random rough surfaces. Such as earth observation (both oceanic and continental surfaces remote sensing), military operations, communications, and also in optical domain. Electromagnetic scattering at various bands from these objects usually contains information about their geometry and properties, which can be exploited by microwave remote sensing. As a noninvasive technique, microwave remote sensing is extremely attractive for this purpose.

This chapter recalls the basic necessary concepts for dealing with electromagnetic wave scattering from random rough surfaces, by using integral equations. First, it recalls the notions of radar equation, Maxwell equations, plane wave propagation, Snell-Descartes laws. Second, it presents an introduction about solutions of scattering equations (Green's function), and how to use Huygens principle and extinction theory to introduce solution for electromagnetic wave scattering, and then provide discussion about far field and normalized radar cross section. Finally, it gives a literature review about asymptotic models for rough surface scattering techniques like: Kirchoff Approximation (KA), Geometric Optics (GO), Small Petrupation Method (SPM) , and Small Slop Approximation (SSA).

1.1 Introduction and Basic Principles

The incident wave illuminating the surfaces will be considered as a plane wave. A wave can be called locally plane if it is located in the so-called Fraunhofer zone[1] [5], of the transmitter source, or far-field zone of the source. This assumes that the source is far enough from the surface such that the incident wave may appear as a plane on a distance greater than any dimension of the surface. The media are assumed to be linear, homogeneous and isotropic (LHI)[2], stationary and non-magnetic. The incident medium is perfectly dielectric [3], and can be assimilated to vacuum in general, although we will trying to write the equations in the general case of any lossless perfect dielectric medium.

The problem of electromagnetic (EM) wave scattering from non-flat surfaces, called rough surfaces, has been studied for decades. Among rough surfaces, two main categories may be distinguished: periodic surfaces (such as square surfaces, triangular surfaces, sawtooth surfaces and sinusoidal surfaces), which are deterministic, and random surfaces for which only some statistical features are known. This chapter aims at introducing the main necessary concepts for understanding the tools used in the following chapters.

[1] The Fraunhofer zone or far-field zone corresponds to a distance R from the source which is greater than approximately $2D^2/\lambda$, where D is the greatest dimension of the source and λ is the transmitted electromagnetic wavelength

[2] The linearity characterizes the fact that the quantities ϵ and μ are independent of the intensity of $\mathbf{E}$ and $\mathbf{H}$, the homogeneity that ϵ and μ do not depend on the considered space point and the isotropy that, μ and σ are scalar

[3] A dielectric medium is called perfect if the considered dielectric medium does not have sources of load or current

1.2 Maxwell's Equations

In their local form, the Maxwell's equations in dielectric media are given by [6], [2]:

$$\text{(Gauss Magnetic Equation)} \quad \boldsymbol{\nabla} \,.\, \mathbf{B} = 0 \tag{1.1}$$

$$\text{(Faraday Equation)} \quad \boldsymbol{\nabla} \times \mathbf{E} = -\frac{\partial \mathbf{B}}{\partial t} \tag{1.2}$$

$$\text{(Gauss Electric Equation)} \quad \boldsymbol{\nabla} \,.\, \mathbf{D} = \rho \tag{1.3}$$

$$\text{(Ampers Law)} \quad \boldsymbol{\nabla} \times \ \mathbf{H} = \mathbf{J} + \frac{\partial \mathbf{D}}{\partial t} \tag{1.4}$$

The vectors $\mathbf{E}$ and $\mathbf{H}$ denote here the electric and magnetic field vectors, expressed in V/m and in A/m. They together form the electromagnetic field. The symbol ∇ is the operator defined in the system of orthogonal coordinates (Cartesian, cylindrical, spherical coordinates, etc.) associated with the coordinate system in which the Maxwell equations are applied. It should be pointed out that in this manuscript the vectors will be denoted in bold, the unit vectors in bold and with a hat and the matrices will be marked in bold and topped with a bar. $\mathbf{D}$ and $\mathbf{B}$ denote respectively the electric displacement and magnetic induction vectors, expressed in C/m^2 and in Tesla [2]. The equation (1.1) and equation (1.2) express the law of induction. Equation (1.3) and equation (1.4) which connect the electromagnetic field ($\mathbf{E,\ H}$) to the sources ($\rho, \mathbf{J}$), respectively represent the densities of charge in (C/m^3) and current in (A/m^2) of the material environment. Indeed, $\mathbf{D}$ and $\mathbf{B}$ are linked to the electric and magnetic fields by constitutive relations

taking account of the medium (vacuum, dielectric material, etc.) [7]. They check the charge conversation equation:

$$\frac{\partial \rho}{\partial t} + \boldsymbol{\nabla}.\mathbf{J} = 0 \tag{1.5}$$

If the media considered linear homogeneous and isotropic (LHI), these relations are expressed as [6]:

$$\mathbf{D} = \epsilon \mathbf{E} = \epsilon_0 \epsilon_r \mathbf{E} \tag{1.6}$$

$$\mathbf{B} = \mu \mathbf{H} = \mu_0 \mu_r \mathbf{H} \tag{1.7}$$

$$\mathbf{J} = \sigma \mathbf{E} \tag{1.8}$$

Where ϵ, μ and σ are, respectively, the permittivity, the permeability and the conductivity of considered matter, with ϵ_0 and μ_0 as their constants in vacuum, which are equal to:

$$\epsilon_0 = \frac{1}{36\pi \star 10^9} F/m \tag{1.9}$$

$$\mu_0 = 4\pi \star 10^- 7 H/m \tag{1.10}$$

These two quantities check the relation: $\epsilon_0 \mu_0 c^2 = 1$, where c, is the light propagation speed in free space, ϵ_r and μ_r are the relative electric permittivity and magnetic permeability, respectively: they are equal to 1 in vacuum. Let us recall that in the following, only non-magnetic media will be considered; consequently, the relative magnetic permeability $\mu_r = 1$. Moreover, propagation media will be assumed to be free of charge, $\rho = 0$, and most of

the time free of current as well, $\mathbf{J} = 0$. A medium that is free of charge is then considered as a dielectric medium; a distinction will be made between a dielectric medium free of current, which will be called perfect dielectric medium or lossless dielectric medium and a dielectric medium not free of current, which will be called lossy dielectric medium.

1.3 Propagation of a Plane Wave (Helmholtz equation)

The propagation of electromagnetic waves is described by the equations of Maxwell. Considering an LHI medium in the presence of charges and current ($\rho \neq 0$ and $\mathbf{J} = \sigma_c \ \mathbf{E} \neq 0$) from the four Maxwell equations of the relations (1.6) and (1.7) the propagation equations of fields are obtained from the Maxwell equations by using the property $\nabla \times (\nabla \times) = \nabla(\nabla .) - \nabla^2$, where ∇^2 is the vector Laplacian[4]. Then, in a general way, we obtain [6], [7]:

$$\boldsymbol{\nabla}^2\mathbf{E} - \epsilon\mu\frac{\partial^2\mathbf{E}}{\partial t^2} - \mu\sigma_c\frac{\partial\mathbf{E}}{\partial t} = \frac{1}{\epsilon}\boldsymbol{\nabla}\rho \tag{1.11}$$

$$\boldsymbol{\nabla}^2\mathbf{H} - \epsilon\mu\frac{\partial^2\mathbf{H}}{\partial t^2} - \mu\sigma_c\frac{\partial\mathbf{H}}{\partial t} = 0 \tag{1.12}$$

For a perfect dielectric medium ($\rho = 0, \mathbf{J} = 0$), the equations reduce to:

$$\boldsymbol{\nabla}^2\mathbf{E} - \epsilon\mu\frac{\partial^2\mathbf{E}}{\partial t^2} = 0 \tag{1.13}$$

$$\boldsymbol{\nabla}^2\mathbf{H} - \epsilon\mu\frac{\partial^2\mathbf{H}}{\partial t^2} = 0 \tag{1.14}$$

[4]In Cartesian coordinates, if we represent the scalar Laplacian by $\triangle = \frac{\partial^2}{\partial x^2} + \frac{\partial^2}{\partial y^2} + \frac{\partial^2}{\partial z^2}$ the vector Laplacian of $\mathbf{A} = A_x, A_y, A_z, \nabla^2\mathbf{A} = \Delta A_x\hat{x} + \Delta A_y\hat{y} + \Delta A_z\hat{z}$

In a general way, the solution of the propagation equation in a perfect dielectric medium for a Plane Progressive Wave (PPW), which propagates in the direction ($\hat{\mathbf{u}} = \frac{\mathbf{R}}{\|\mathbf{R}\|}$) at speed v, is written as [6]:

$$\Psi = \Psi_+(t - \frac{\hat{\mathbf{u}}.\mathbf{R}}{v}) + \Psi_-(t + \frac{\hat{\mathbf{u}}.\mathbf{R}}{v}) \tag{1.15}$$

Where, by definition of the plane wave, the wave planes (or surfaces of the plane waves) are orthogonal to $\hat{\mathbf{u}}$ defined by the planes $\hat{\mathbf{u}}.\mathbf{R} = C$, where C is a constant. The function Ψ_+, sometimes called PPW_+, is a a progressive wave that propagates at speed v in the direction $+\mathbf{R}$. Likewise, Ψ_-, sometimes called PPW_-, is a progressive wave that propagates at speed v in the direction $-\mathbf{R}$. This wave function is checked by both $\mathbf{E}$ and $\mathbf{H}$, and it can be shown that:

$$\mathbf{H} = Z\hat{\mathbf{u}} \times \mathbf{E} \tag{1.16}$$

Where $Z = \sqrt{\frac{\mu}{\epsilon}} = Z_0\sqrt{\frac{\mu_r}{\epsilon_r}}$ is the wave impedance of the considered medium, with Z_0 the wave impedance of vacuum which is equal to $Z_0 = \sqrt{\frac{\mu_0}{\epsilon_0}} = 120\pi$. Thus, **(E, H, $\hat{\mathbf{u}}$)** form a direct trihedral. The wave is then called transverse electromagnetic (TEM), because both vectors $\mathbf{E}$ and $\mathbf{H}$ are orthogonal to the propagation direction given by $\hat{\mathbf{u}}$. A harmonic plane progressive wave (HPPW) is a space-time function of real expression, after take the real part of exponential $e^{i\omega(t-\frac{\hat{\mathbf{u}}.\mathbf{R}}{v})-\phi}\hat{\mathbf{\Psi}}$ [2].

$$\mathbf{\Psi}(\mathbf{R},t) = A\cos\{\omega(t - \frac{\hat{\mathbf{u}}.\mathbf{R}}{v}) - \phi\}\hat{\mathbf{\Psi}} = A\cos(\omega t - \mathbf{k}.\mathbf{R} - \phi)\hat{\mathbf{\Psi}} \qquad (1.17)$$

Where $\mathbf{k} = (\omega/v)\hat{\mathbf{u}}$ is the wave vector, ω is the pulsation in rad/s and ϕ is a constant phase term. In the following, we will consider the harmonic regime such that every EM quantity is an HPPW of complex form:

$$\mathbf{\Psi}(\mathbf{R},t) = A\exp[\pm i(\omega t - \mathbf{k}.\mathbf{R} - \phi)]\hat{\mathbf{\Psi}} = \Psi(\mathbf{R})\exp(\pm i\omega t)\hat{\mathbf{\Psi}} \qquad (1.18)$$

where $\Psi(\mathbf{R}) = \exp[\pm i(\mathbf{k}.\mathbf{R} + \phi)]$. Depending on the sign convention + or − in $\exp[\pm i(\omega t - \mathbf{k}.\mathbf{R})$, the time derivative operator $\frac{\partial}{\partial t}$ is equivalent to a multiplication by $\pm i\omega$ and the space derivative operator $\nabla.$ is equivalent to a multiplication by $\pm i\mathbf{k}$.

In the following, the retained convention is $\exp[-i(\omega t - \mathbf{k}.\mathbf{R})]$. Thus, the wave equation (1.13) of the electric field $\mathbf{E}(\mathbf{R},t) = \mathbf{E}_0(\mathbf{R})\exp(\pm i\omega t)$ in a free of charge and current medium becomes:

$$(\boldsymbol{\nabla}^2 + k^2)\mathbf{E} = 0 \qquad (1.19)$$

with $k^2 = \omega^2/v^2$(dispersion relation), where k represents the wavenumber inside the considered perfect dielectric medium. This equation, which is called the *Helmholtz equation*, is also checked by the magnetic field $\mathbf{H}$.

By taking the surface currents $\mathbf{J} = \sigma\mathbf{E}$ into account, the wavenumber k is expressed by the dispersion relation as [7]:

$$k^2 = \frac{\omega^2}{v^2}(1 + i\frac{\sigma}{\omega\epsilon}) \tag{1.20}$$

In this case, the wavenumber k is complex and the wave is damped during its propagation inside the lossy medium. The time convention $e^{(-j\omega t)}$ is omitted throughout this work.

1.4 Boundary condition

Every medium is by nature finite, bounded by at least one different medium. It is therefore important to characterize the behavior of the waves at the boundary of the two media. Thus, new equations valid at the interface with another medium must be established. These equations, obtained from Maxwell's equations. Consider the scene presented in Figure 1.1. A surface S separates a medium (1) from a medium (2) and $\hat{\mathbf{n}}$, the normal at S , is oriented from (2) to (1).

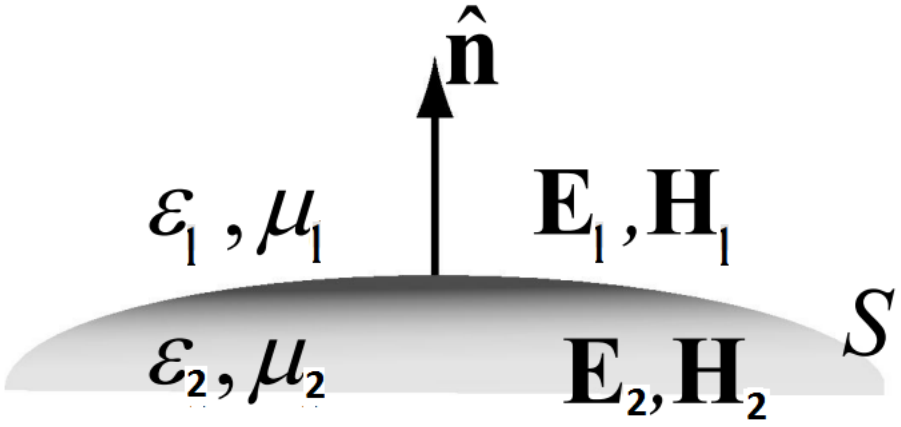

Figure 1.1: Interface between two semi-infinite LHI media

The Boundary conditions (also referred to as continuity relationships) are expressed:

$$\hat{\mathbf{n}} \quad . \quad (\mathbf{B}_2 - \mathbf{B}_1) = 0, \tag{1.21}$$

$$\hat{\mathbf{n}} \quad . \quad (\mathbf{D}_2 - \mathbf{D}_1) = \rho_s, \tag{1.22}$$

$$\hat{\mathbf{n}} \times (\mathbf{E}_2 - \mathbf{E}_1) = 0, \tag{1.23}$$

$$\hat{\mathbf{n}} \times (\mathbf{H}_2 - \mathbf{H}_1) = \mathbf{j}_s, \tag{1.24}$$

Where ρ_s and $\mathbf{J}_s$ represent the surface density of charge and the vector of superficial (or surface) density of current, respectively, which may exist at the boundary between the two media ($\rho_s = 0$ for dielectric media, $\rho_s = 0$ and $\mathbf{J}_s = 0$ for perfect dielectric media). Equations (1.21) and (1.23), called continuity relations, describe the continuity of the normal component of $\mathbf{B}$ and of the tangential component of $\mathbf{E}$ at the interface, respectively. The other two equations (1.22) and (1.24) describe the discontinuity of the normal component of $\mathbf{D}$ in the presence of surface charges of density ρ_s and the discontinuity of the tangential component of $\mathbf{H}$ on a layer of current, respectively. Using the same method, for the case when the two LHI media are perfect dielectric, the equations take the form:

$$\hat{\mathbf{n}} \quad . \quad (\mathbf{B}_2 - \mathbf{B}_1) = 0 \tag{1.25}$$

$$\hat{\mathbf{n}} \quad . \quad (\mathbf{D}_2 - \mathbf{D}_1) = 0 \tag{1.26}$$

$$\hat{\mathbf{n}} \times (\mathbf{E}_2 - \mathbf{E}_1) = 0 \tag{1.27}$$

$$\hat{\mathbf{n}} \times (\mathbf{H}_2 - \mathbf{H}_1) = 0 \tag{1.28}$$

1.5 Polarizations

The plane of incident is formed by the wave vector incident onto the surface $\hat{\mathbf{k}}_i$ and the normal to the surface $\hat{\mathbf{n}}$. In the case when the studied surface is flat, $\hat{\mathbf{n}} \in (\hat{\mathbf{x}}, \hat{\mathbf{z}})$ with constant direction whatever the surface point, the incidence plane $(\hat{\mathbf{k}_i}, \hat{\mathbf{n}})$ is identical to the plane $(\hat{\mathbf{x}}, \hat{\mathbf{z}})$ as illustrated in Figure 1.2. In the case of a rough surface, the normal to the surface becomes a local normal that depends on the considered surface point.

Considering an arbitrary rough surface for which the height η depends on the two horizontal parameters x and y,$\eta(x, y)$, the normal does not belong to the plane $(\hat{\mathbf{x}}, \hat{\mathbf{z}})$, then the incidence plane depends on the considered surface point. For better convenience, the polarization of the incident wave is defined relatively to the mean plane $(\hat{\mathbf{k}_i}, \hat{\mathbf{n}})$ as illustrated in Figure 1.2.

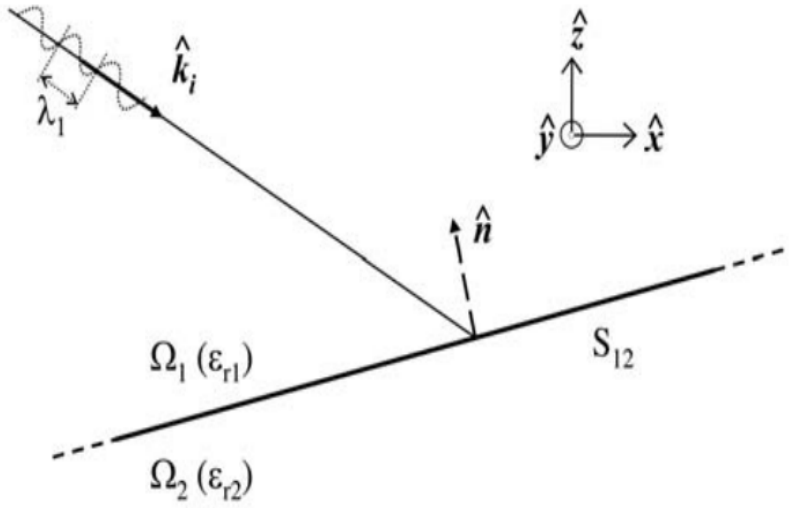

Figure 1.2: Incident wave on an infinite flat surface: cut view in the incidence plane ($\hat{\mathbf{k}}_i$,$\hat{\mathbf{n}}$)

To study the polarization in the general case rigorously, it is necessary to con-

sider an arbitrary elliptical polarization. However, by considering a cartesian coordinate system and knowing that every polarization state of a wave can be represented by the combination of two linear horizontal and vertical components, we will study these two fundamental components.

A possible representation of the horizontal and vertical polarizations is given in Figure 1.3 and Figure 1.4. Note that in the literature, various denominations of these polarizations are given: the horizontal (denoted by H) polarization is also called the transverse electric (denoted by TE) polarization or perpendicular polarization. The vertical (denoted by V) polarization is also called the transverse magnetic (denoted by TM) polarization or parallel (denoted by P for parallel in the optical domain) polarization.

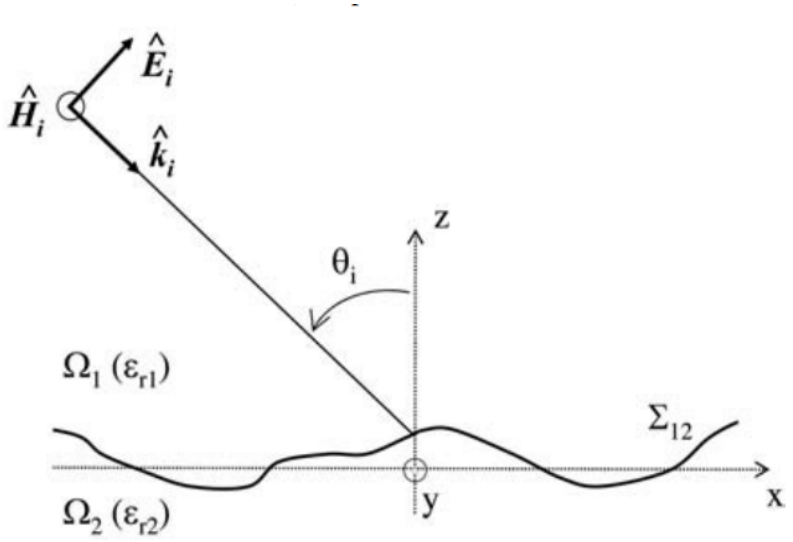

Figure 1.3: Incident wave onto a random rough interface in horizontal (H) polarizations: cut view in the mean incidence plane ($\hat{\mathbf{k}}_i$,$\hat{\mathbf{z}}$) [2].

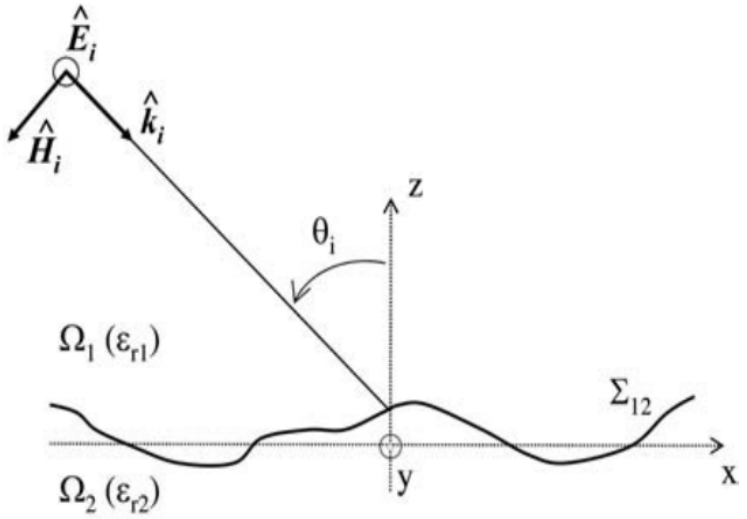

Figure 1.4: Incident wave onto a random rough interface in vertical (V) polarizations: cut view in the mean incidence plane ($\hat{\mathbf{k}}_i$,$\hat{\mathbf{z}}$)

1.6 Green's function

The solution for EM differential equation called Green's function. Each component of $\mathbf{E}$ checks the propagation equation, in scalar where the operator $(\triangle + k^2)$. Greens function associated with these operator checks [6]:

$$(\triangle + k^2)G(\mathbf{R}, \mathbf{R}') = -\delta(\mathbf{R}, \mathbf{R}'). \tag{1.29}$$

It's seen that the Green's function always depends on the source and observation vectors defined $(\boldsymbol{R}', \mathbf{R})$ respectively. It corresponds physically to the radiation of a point source. Finally the solution of equation (1.29) for 3D scattering is [7]:

$$G(\mathbf{R},\mathbf{R}') = \frac{e^{ik\|\mathbf{R}-\mathbf{R}'\|}}{4\pi \parallel \mathbf{R}-\mathbf{R}' \parallel}. \tag{1.30}$$

Then the solution of the integral equation is the convolution of EM waves and Greens function. In order to obtain the integral representation, it's necessary to transform an integral volume form into surface integral form using Ostogrdski's theorem [13]:

$$\int\int\int_V [\mathbf{Q}.(\nabla\times\nabla\times\mathbf{P}) - \mathbf{P}.(\nabla\times\nabla\times\mathbf{Q})]dv = \int\int_S [\mathbf{P}\times(\nabla\times\mathbf{Q}) - \mathbf{Q}\times(\nabla\times\mathbf{P})].\hat{\mathbf{n}}ds. \tag{1.31}$$

Where S is a surface delimiting a volume V and $\hat{\mathbf{n}}$ is the normal to the surface S directed towards outside the volume V. $\mathbf{P}$ and $\mathbf{Q}$ are two vector functions of the point (also called vector field or any vector field), at any point belonging to volume V or surface S.

1.7 Huygens principle and extinction theory

The Huygens principle [2], [7] is a fundamental principle of the theory of light. Huygens' principle is based on the fact that each point of a wavefront is itself a radiation source of a wave. By this principle, a source of radiation can be replaced by a set of sources. These currents are placed on a surface closed arbitrary encompassing the original source. This theorem allows us to describe radiation from a current distribution on a surface, or to obtain a surface integral equation of the currents induced on an object excited by a incident field.

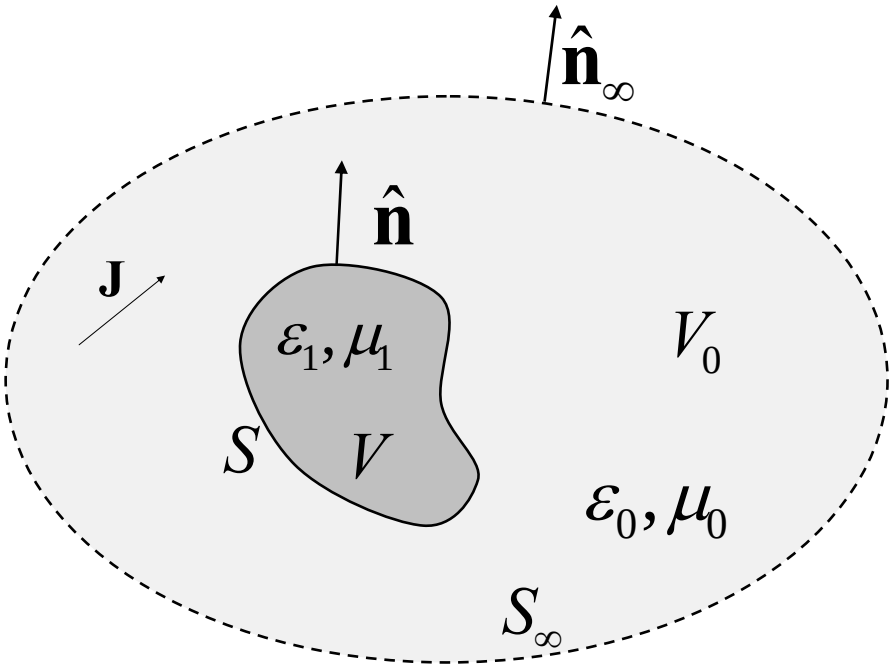

Figure 1.5: Geometry of the Scattering Problem

Consider the scene presented in Figure 1.5. A source **J** is placed in a medium Ω_0 of permittivity ϵ_0 and permeability μ_0 containing a medium object Ω_1 of permittivity ϵ_1 and permeability μ_1. S is the surface delimiting the volume V and its normal, $\hat{\boldsymbol{n}}$, is directed towards the outside of V (thus directed towards the interior of V_0). Where is the surface delimiting the volume V_0 at infinity and its normal point outward of V_0. From equation (1.31) applied at volume V_0, and Maxwell's equations, the following equation is obtained [7].

$$\begin{cases} \mathbf{E}(\mathbf{R}'), & \text{if} \quad \mathbf{R}' \in \text{ V}_0 \\ 0, & \text{otherwise} \end{cases} = \mathbf{E}_i(\mathbf{R}') + \int\int_S [G(\mathbf{R},\mathbf{R}')i\omega\mu(\hat{\mathbf{n}}(\mathbf{R}) \times \mathbf{H}(\mathbf{R})) + (\hat{\mathbf{n}}(\mathbf{R}) \times \mathbf{E}(\mathbf{R})) \times \nabla G(\mathbf{R},\mathbf{R}') + (\hat{\mathbf{n}}(\mathbf{R}).\mathbf{E}(\mathbf{R}))\nabla G(\mathbf{R},\mathbf{R}')]ds. \tag{1.32}$$

when $\mathbf{R}'$ not belong V_0 the equation (1.32) becomes :

$$\mathbf{E}_i(\mathbf{R}') = -\int\int_S [G(\mathbf{R},\mathbf{R}')i\omega\mu(\hat{\mathbf{n}}(\mathbf{R})\times\mathbf{H}(\mathbf{R}))+ \\ (\hat{\mathbf{n}}(\mathbf{R})\times\mathbf{E}(\mathbf{R}))\times\nabla G(\mathbf{R},\mathbf{R}') + (\hat{\mathbf{n}}(\mathbf{R}).\mathbf{E}(\mathbf{R}))\nabla G(\mathbf{R},\mathbf{R}')]ds. \tag{1.33}$$

This equation is known as the extinction vector theorem of Ewald-Oseen [14], and imposes the cancellation of the total field inside the object of volume V; the incident field being compensated by the contribution of the surface fields. By defining the total field $\mathbf{E}$ as the sum of $\mathbf{E}_i$, the incident field and $\mathbf{E}_{sr}$ the diffracted field (scattered field), equation (1.32) becomes in the volume V_0 :

$$\mathbf{E}_{sr}(\mathbf{R}') = \int\int_S [G(\mathbf{R},\mathbf{R}')i\omega\mu(\hat{\mathbf{n}}(\mathbf{R})\times\mathbf{H}(\mathbf{R})) + (\hat{\mathbf{n}}(\mathbf{R})\times\mathbf{E}(\mathbf{R}))\times\nabla G(\mathbf{R},\mathbf{R}')+ \\ (\hat{\mathbf{n}}(\mathbf{R}).\mathbf{E}(\mathbf{R}))\nabla G(\mathbf{R},\mathbf{R}')]ds. \tag{1.34}$$

This equation is known as the Huygens Principle and allows the propagation of surface fields outside volume V, forming the total field after summation with the incident field. If the object of volume V is dielectric, the field is not necessarily zero for $\mathbf{R}'$ not belong to V_0, from the curl relations, this time applied to volume V, we obtain a new equation

$$\begin{cases} \mathbf{E}(\mathbf{R}'), & if \quad \mathbf{R}' \in \text{ V} \\ 0, & \text{otherwise} \end{cases} = -\int\int_S [G_1(\mathbf{R},\mathbf{R}')i\omega\mu(\hat{\mathbf{n}}(\mathbf{R}) \times \mathbf{H}(\mathbf{R})) + \tag{1.35}$$

$$(\hat{\mathbf{n}}(\mathbf{R}) \times \mathbf{E}(\mathbf{R})) \times \nabla G_1(\mathbf{R},\mathbf{R}') + (\hat{\mathbf{n}}(\mathbf{R}).\mathbf{E}(\mathbf{R}))\nabla G_1(\mathbf{R},\mathbf{R}')]ds.$$

where $G_1(\mathbf{R},\mathbf{R}')$ is the function of Green . For $\mathbf{R}'$ belong to V, the equation (1.43) shows the principle of Huygens applied in volume V; for $\mathbf{R}'$ not belong to V, we recognize the expression of the extinction theorem. Thus, equation (1.35) imposes the cancellation of the radiated field towards the outside of the object and makes it possible to calculate the total field in the object. So the problem has been broken down into two parts, one looking for equivalent sources creating the total field in volume V_0 and the other looking for equivalent sources creating the total field in volume V (equation (1.35)).

1.8 Radar Cross Section and Scattering Coefficient

The measure of the ability of a target to reflect radar signal in the direction of the radar receiver is known as Radar Cross Section (RCS). If the incident signals were reflected uniformaly in all direction, then the RCS is equal to the cross-sectional area of a target seen by the transmitter [16].

RCS has been defined to characterize the target characteristics and not the effects of transmitter power, receiver sensitivity, and position of the transmitter or receiver distance.

1.8.1 IEEE RCS Definition

The IEEE dictionary of electrical and electronics defines RCS (σ) as a measure of reflective strength of a target defined as 4π times the ratio of the power per unit solid angle scattered in a specified direction to the power per unit area in a plane wave incident on the scatterer from a specified direction. More precisely, it is the limit of that ratio as the distance from the scatterer to the point where the scattered power is measured approaches infinity [22]:

$$\sigma = \lim_{r \to \infty} 4\pi r^2 \frac{\|\mathbf{E}_s\|^2}{\|\mathbf{E}_i\|^2}, \tag{1.36}$$

where $\mathbf{E}_s$ is the scattered electric field and $\mathbf{E}_i$ is the field incident at the target. Three cases are distinguished: monostatic or backscatter, forward scattering, and bistatic scattering. Bistatic cross section is for the case when the transmitter and receiver are at different locations.

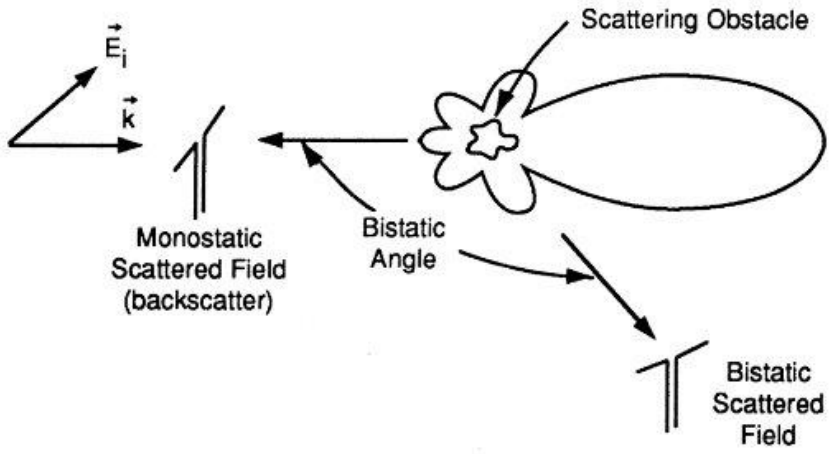

Figure 1.6: Monostatic and Bistatic scattering [22]

Forward cross section is a measure of scattered power in forward direction; that is, in the same direction as the incident field. This forward scattered

power is usually 180^0 out of phase with the incident field so that when added to the incident field a shadow region is formed behind the scattering object. Monostatic or backscatter cross section is the radar systems where the receiver and transmitter are collocated, often times using the same antenna for transmitting and receiving.

1.9 Literature Review: Computational Models [2],[7]

When studying the wave scattering from random rough surfaces, the problem of predicting the surface is encountered. In some cases, it is possible to know it exactly. For rough surfaces with spatial variations but not with time variations. For space- and time-varying surfaces, the problem is different a priori, as the surface varies with time. For instance, for sea surfaces, sensors located on buoys are used. Then, by assuming a stationary process, the knowledge of some statistical features of the surface makes it possible to describe the stochastic random rough surface: usually, it is the height probability density function (PDF) and the height autocorrelation function [2].

The resolution of the problem of scattering from such surfaces then implies determining the surface currents on the random rough surface. Models called rigorous models make it possible to resolve the problem without any approximation on a parameter of the surface. For the case of scattering from random rough surfaces, the analytical methods do not make it possible to resolve the problem without approximation. Only numerical methods, for which the surface is discretized, make it possible to resolve the problem with-

out approximation. They are based on the resolution of the local Maxwell equations on the surface. These methods are usually qualified as "exact "or simply "rigorous", as the discretization has an influence on the precision of the result.

These rigorous models resolved by numerical methods have the advantage of being exact, but in return they require, in general, a long computation time and a large memory space. Thus, it is of interest to use asymptotic models, which have the great advantage of being faster to compute. Because of their complexity, the rigorous models usually allow us to treat surfaces with restricted dimensions (typically, $30\lambda \times 30\lambda$ for 3D problems).

The asymptotic models usually allow us to treat larger surfaces. However, as their name implies, asymptotic models are applicable only in a restricted validity domain. Indeed, for resolving the problem more easily and/or more rapidly, simplifying hypotheses must be used. Most of the time, these hypotheses rest on a parameter of the random rough surface, which must be less or more than a parameter of the incident and/or scattered wave. For simple asymptotic models, it is usually the height (RMS) σ_h relative to the wavelength λ. If $\sigma_h << \lambda$, the model is of low-frequency type; on the contrary, if $\sigma_h > \lambda/4$, the model is of high-frequency type.

Other surface parameters may also be involved, such as the mean surface curvature radius R_c relative to the wavelength λ, the RMS slope σ_s relative to the slopes of the incident and scattered waves or, similarly, the correlation length L_c relative to the wavelength λ; moreover, several of these hypotheses may combine. In order to study the validity of an asymptotic model, it is

useful to compare the results with a rigourous model. This will permit to study the limits and the validity domain of the asymptotic model.

1.9.1 Rigorous models

All rigorous models that deal with random rough surface scattering use numerical techniques. These methods can be divided into two main categories: differential methods and integral methods. Differential (or volumetric) methods are based on a problem of a partial differential equation. They require a meshing of the space (3D meshing for a 3D problem, 2D meshing for a 2D problem) whose shape and sampling step must be chosen carefully, depending on the studied problem and on the desired precision. These methods are of finite element type, such as the finite element method (FEM), for which the problem is formulated in the frequency domain, and the methods of finite difference type, such as the finite difference time domain (FDTD) technique, for which the problem is formulated in the temporal domain [2]. The latter methods are of interest for heterogeneous media.

As their name implies, the integral methods start from integral equations of the field on the surface. In the frequency domain, the integral equations are sampled in order to solve the problem. For doing so, the Method of Moments (MoM) is often used. Then, the problem is transformed into a matrix, and the difficulty lies in its inversion. It may be made directly; still, for computing time and memory space constraints, it is better to optimize this inversion. Thus, iterative methods are often used: the fast multipole method (FMM) [9], the banded matrix iterative approach/ canonical grid (BMIA/CAG) [11],

the multilevel fast multipole (MLFMM) [8], the forward-backward method (FB) [7], the method of ordered multiple interactions (MOMI) [10] and so on .

1.9.2 Asymptotic models

Asymptotic models may use either numerical or analytical resolution methods. Typically, numerical asymptotic methods were developed to resolve complex problems that the exact numerical methods could either hardly resolve, or only by means of extensive computing time and/or memory space. This is the case, for instance, of ray tracing and ray launching methods [15]. Moreover, classical asymptotic models, which are generally solved by analytical methods, may also be resolved numerically.

For instance, let us quote the methods based on KA [20] and the Small Perturbation Method SPM [15]. As discussed earlier in the introduction, in general, simple asymptotic models may be split up into two main categories: low-frequency and high-frequency models. A third category gathers the asymptotic models that aim at being applicable to both low and high frequencies: these models are then qualified as unified.

After, we will give a panorama of the different categories of models. Then, the models taking the phenomenon of multiple scattering will not be presented, and a summary of the validity domains of simple asymptotic models will be given, the first developed model is a low-frequency model: the SPM, which is sometimes called Bragg scattering theory. Its pioneer was Lord Rayleigh [21] who treated the case of sinusoidal surfaces. The SPM may be considered

as a series expansion of the scattered field depending on the surface heights. It was developed at orders 1 and 2, before being completed by Peake [16]. Johnson et al [19], developed the model up to order 3, and then up to order 4. The higher the surface RMS height is, the higher the order of SPM must be considered for the model to be valid [4]. For the first order of SPM (denoted SPM1), the normalized radar cross-section (NRCS) (or scattering coefficient) is proportional to the surface height spectrum. Usually, SPM1 is considered to be valid for RMS heights σ_h and RMS slopes σ_s as shown in Figure 1.7 checking [4]:

$k_0\sigma_h < 0.3$, and $\sigma_s < 0.3$, where k_0 is the wavenumber inside the incidence medium, which is vacuum.

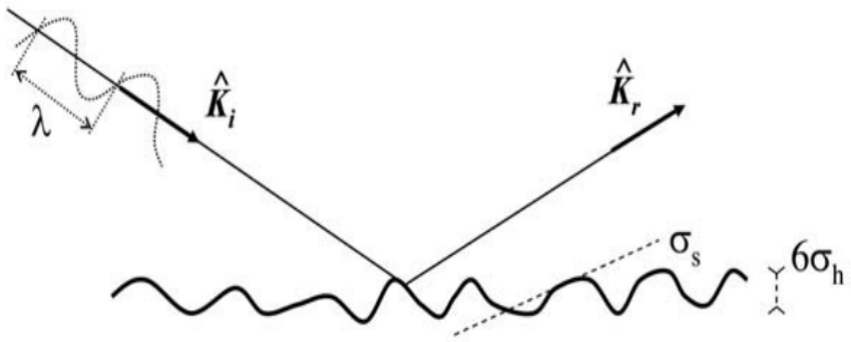

Figure 1.7: Random rough surface of SPM1 type [2]

The most often used and best-known high-frequency method is the KA. Usually called the Kirchhoff Approximation in short, or Physical Optics (PO) approximation by numericians and/or in the radar scattering community [2],

it assumes that the wavelength is (much) less than the mean surface curvature radius R_c ($R_c > \lambda$): the surface is then locally smooth (flat). It is also necessary that the wavelength be less than the surface correlation length, $L_c > \lambda$. Thus, locally, at each surface point, the surface can be replaced by its tangent plane, which is a flat surface whose local slope is equal to the slope of the original random rough surface at the considered surface point. As a result, each ray of the incident wave is reflected (or transmitted) specularly by the tangent plane at each rough surface point. This method depends only on the Fresnel reflection (or transmission) coefficient evaluated at the considered local incidence angle for giving the amplitude, and on the appropriate Snell−Descartes law for giving the direction of the reflected (or transmitted) wave. Note that, however, this model diverges for low-grazing incidence angles, because of the shadowing phenomenon of the surface; that is why, it is necessary to introduce a corrective parameter called shadowing function which is added to KA (or sometimes illumination function) to overcome this issue.

The Geometric Optics (GO) approximation was introduced by Eckart [7], who was the first to demonstrate that, with this high-frequency approximation for which the RMS height checks $\sigma_h > \lambda/4$, the scattering coefficient (or NRCS) is proportional to the surface slope. More precisely, the GO is applicable if the wavelength is much lower than any parameter of the surface. Then, for a flat surface, the surface parameters are its length and width L_x and L_y, respectively. For a random rough surface, the height variations must be taken into account through the RMS height σ_h; also, its other characteristic

dimensions should not be forgotten: in particular, the mean curvature radius R_c and also the correlation length σ_s shown in Figure 1.8.

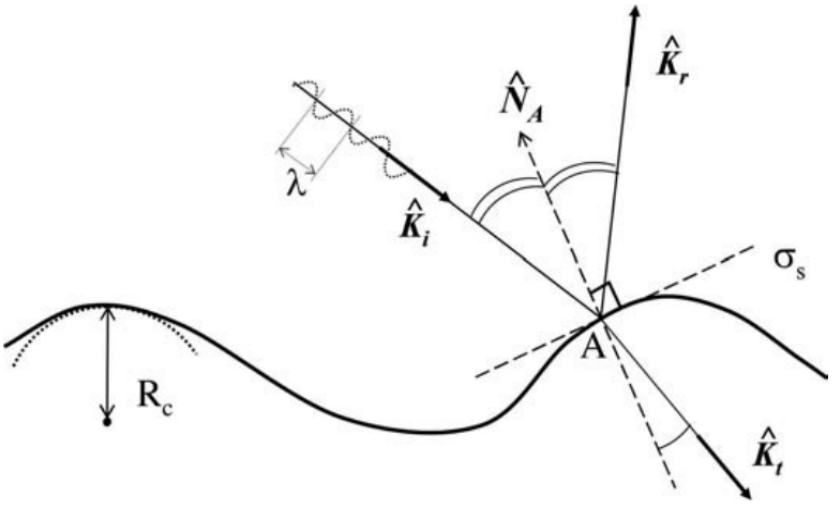

Figure 1.8: Random rough surface of KA type [2]

In the rough surface scattering community, the KA is not used as such; its mathematical expression is simplified in order to obtain faster numerical results. Method of Stationary Phase (MSP) [2] is used very commonly; this approximation implies the following assumption: $\sigma_h > \lambda/A$ with $A > 4$ a constant.

Physically, it assumes that, for given incidence and observation directions, the points of the surface that contribute to the scattering process are the points that reflect the incident wave specularly into the observation direction. This comes from the fact that the phase term inside the integral to be computed oscillates very rapidly; then, the main contribution of the integrand can be represented by the points for which the phase of the integrand is stationary (i.e. null derivative of the phase). This corresponds to a commonly called

saddle-point technique, and it may be assimilated physically to retain only the envelope of the function (signal). As a result, the slope of the surface points, which contribute to the scattering process, depends only on the angles of incidence and observation: the dependence on the slopes in the integral is suppressed, which makes it possible to greatly simplify the calculation of the statistical moments.

Moreover, in order to get rid of the dependence on the surface heights, which appear inside the phase term of the scattered intensity (or power), the GO may also be used as a further approximation. From a qualitative point of view, the associated constraint is the same as for the MSP, but it is a bit stronger ($\sigma_h > \lambda/B$, with B also a constant checking $B < A$): it is applicable to even rougher surfaces. In fact, $\sigma_h > \lambda/4$ ($B = 4$) is generally enough.

After we made a revision and introduction to concept and models used in EM scattering, we will then focus and develop one asymptotic model in next chapter called Kirchhoff approximation (KA) or Physical Optics (PO), we will discuss it in details for 3D rough surface. Starting from applying this technique for a flat surface (plate) and ending by applying it to very rough surface, during that we check the validity of KA and make a comparison between KA and the accelerated method of moments (MOM) which is called Multilevel fast Multipole Method (MLFMM).

Chapter 2

Electromagnetic Scattering from Two Dimensional Rough Surface

---

This chapter describes classical statistical description of random rough surfaces, using the height distribution and autocorrelation function, then it introduces asymptotic models used to evaluate the field scattered by random rough surfaces, focusing on the Kirchhoff-tangent plane Approximation (KA). Their theoretical math model and validity domains are given.

The previous chapter focused on the basic tools necessary for understanding the problem of electromagnetic (EM) wave scattering from surfaces in general, and random rough surfaces in particular. In this chapter, the first section deals with the statistical description of random rough surfaces. The next section introduces the first classification of random rough surface by Rayleigh roughness, after that in section 2.4 will introduce the KA technique.

Finally, the RCS of a plate and random rough surface is calculated using KA and compared to results obtained from the accelerated MOM (MLFMM) obtained from commercial software EM simulator (FEKO).

2.1 Random Rough Surface

Rough surface is a random process $\{\eta = f(x, y)\}$, so we must study its statistical properties such as mean variance autocorrelation between points in the surface; we start to identify the surface by understanding the surface

height profile or Power Distribution Function (PDF). In this work we consider a rough surface with Gaussian distribution, with mean η_0 and standard deviation σ_h .

2.1.1 Statistical Description of Random Rough Surfaces

We shall assume that the profile is defined randomly. The description of a random rough surface with height variations η and surface height PDF $p_h(\eta)$ represents the statistical height distribution of the random rough surface. The probability density of the profiles under consideration will be chosen Gaussian, centered with mean η_0 and standard deviation σ_h, $p_h(\eta)$ is then given by [19]:

$$P_h(\eta) = \frac{1}{\sigma_h\sqrt{2\pi}} \exp\{(-\frac{1}{2}(\frac{\eta - \eta_0}{\sigma_h})^2\} \tag{2.1}$$

and

$$\langle 1\rangle = \int_{-\infty}^{\infty} P_h(\eta)d\eta = 1, \langle \eta\rangle = \int_{-\infty}^{\infty} \eta P_h(\eta)d\eta = 0, \tag{2.2}$$

for simplicity the mean height η_0 will be taken as 0, this averaging of the heights is the statistical moment of order one (average value). The statistical moment of order two, $\langle(\eta - \langle\eta\rangle)^2\rangle = \langle\eta^2\rangle$ (for $\eta_0 = 0$), also called variance, corresponds here to the averaging on the square of the heights [7]. It is written as:

$$\langle\eta^2\rangle = \int_{-\infty}^{\infty} \eta^2 P_h(\eta)d\eta = {\sigma_h}^2, \tag{2.3}$$

Where $\sigma_h = \sqrt{\langle \eta \rangle^2}$, denotes the standard deviation of the profile heights, which is also called root mean square (RMS) height σ_h. Thus for a Gaussian height PDF, 99.73% of the surface heights are contained between $\eta_0 - 3\sigma_h$ and $\eta_0 + 3\sigma_h$ as in Figure 2.1 .

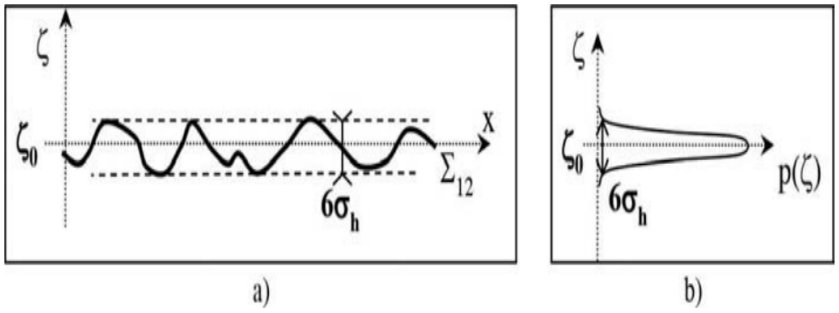

Figure 2.1: One-dimensional (1D) random rough surface of Gaussian statistics, and its height distribution [7]

2.1.2 Surface (spatial) height autocorrelation function and height spectrum

The autocorrelation function between two surface points M_1 and M_2 represents the statistical correlation between these two points, with respect to their horizontal distance $\mathbf{r}_d$=$\mathbf{r}_2$ - $\mathbf{r}_1$. It is maximum if $\boldsymbol{r_2}$= $\mathbf{r}_1$ (or $\mathbf{r}_d$ =0). Two important pieces of information are contained in this function: Its correlation lengths along $\hat{x}$ and $\hat{y}$, $L_{c,x}$ and $L_{c,y}$, and its type: Gaussian, Lorentzian, exponential, etc. It is defined by [7]:

$$\mathbf{W}_h(\mathbf{r}_1, \mathbf{r}_2) = \langle \eta(\mathbf{r}_1)\eta(\mathbf{r}_2) \rangle = \lim_{X,Y \to \infty} \frac{1}{XY} \int_{-\frac{X}{2}}^{\frac{X}{2}} \int_{-\frac{Y}{2}}^{\frac{Y}{2}} \eta(\mathbf{r}_1)\eta(\mathbf{r}_2) dxdy \qquad (2.4)$$

Where X, Y are the surface lengths with respect to ($\hat{\mathbf{x}}$) and ($\hat{\mathbf{y}}$), respectively. For a stationary surface [1], $W_h(\mathbf{r}_1, \mathbf{r}_2)$=$W_h(\mathbf{r}_d)$, with the property $W_h(\mathbf{r}_d = 0)$=${\sigma_h}^2$ when $\mathbf{r}_d = 0$. The autocorrelation coefficient $C(r_d)$ is equal to the autocorrelation function normalized by the RMS height (height standard deviation); it is written for a stationary surface as:

$$C_h(\mathbf{r}_d) = \frac{\langle \eta(\mathbf{r}_1)\eta(\mathbf{r}_1 + \mathbf{r}_d) \rangle}{{\sigma_h}^2} \qquad (2.5)$$

The correlation length L_c is a characteristic value of the autocorrelation function, which determines the so-called scale of roughness of the surface. Typically, it corresponds to the horizontal distance (x_d for $L_{c,x}$ or y_d for $L_{c,y}$) between two surface points for which the autocorrelation coefficient is equal to $1/e$ as in Figure 2.2, provided that the autocorrelation function is taken as Gaussian $W_h(x_d) = {\sigma_h}^2 exp(-\frac{{x_d}^2}{{L_c}^2})$.

[1] In its usual definition, a stationary process is a stochastic process whose first moment and covariance do not change when shifted in time or space. As applied to surfaces, it means that the mean value and the autocorrelation function do not change with respect to space.

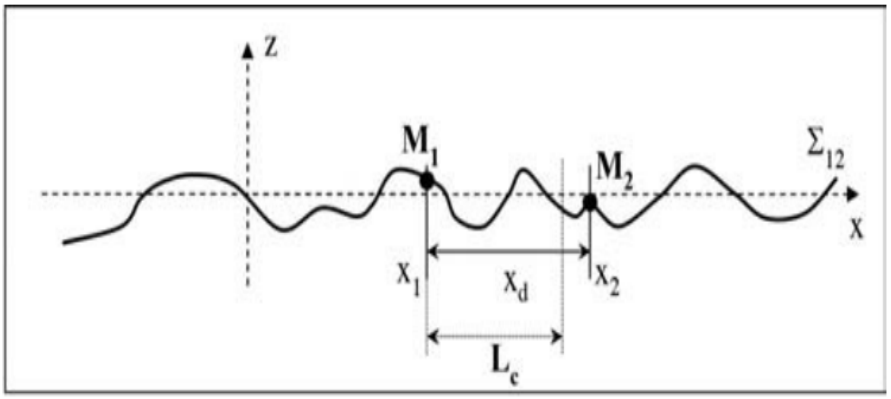

Figure 2.2: 2D random rough surface and its height autocorrelation function [2]

2.1.3 Other Statistical properities [2]

In addition to the RMS height σ_h and the correlation length L_c, other important statistical parameters can be useful to characterize a random rough surface. The first parameter is the surface RMS slope σ_s , which is defined by:

$$\sigma_s = \sqrt{\langle \{\eta\prime - \langle \eta\prime \rangle\}^2 \rangle} \tag{2.6}$$

For a Gaussian PDF surface with Gaussian correlation, the RMS slope is related to the RMS height and the correlation length by $\sigma_s = \sqrt{2}\frac{\sigma_h}{L_c}$. The second commonly used parameter is the surface mean curvature radius R_c, which is defined for 1D surface as:

$$R_c = -\frac{\{1 + \langle \eta\prime(x)^2 \rangle\}^{\frac{3}{2}}}{\langle \eta\prime\prime(x) \rangle} \tag{2.7}$$

For a Gaussian surface (i.e. Gaussian height PDF and Gaussian correlation), under small slopes assumption, the mean curvature radius checks the asymptotic relation, which simplifies for RMS slope $\sigma_s \ll 1$ as:

$$R_c = 0.36\frac{L_c^2}{\sigma_h} \tag{2.8}$$

Sometimes, an additional parameter is used: the mean distance D_m between two successive peaks of the surface. It can be estimated [2]:

$$D_m = \pi\sqrt{\frac{\int_{-\infty}^{\infty} dk k^2 S(k)}{\int_{-\infty}^{\infty} dk k^4 S(k)}} \tag{2.9}$$

Where

$$S(k) = FT\{W_h(\mathbf{r}_1, \mathbf{r}_2)\} = \int_{-\infty}^{\infty}\int_{-\infty}^{\infty} W_h(\mathbf{r}_d)\exp(-i\mathbf{k}.\mathbf{r}_d)d\mathbf{r}_d, \tag{2.10}$$

is power spectrum density of auto correlation function . Physically, it is expected that this distance D_m would be of the same order as the correlation length L_c. Indeed, for a Gaussian surface, this distance checks the condition:

$$D_m = \frac{\pi}{\sqrt{6}}L_c \cong 1.28L_c \tag{2.11}$$

This is consistent with our qualitative physical prediction. Besides, it can be noted that (at least for a Gaussian correlation surface) the distance between two surface peaks is a bit greater than the correlation length.As an example

of rough surface the next Figure 2.3, with $\sigma_h = 0.02, L_c = 1.2, \lambda = 1, \Delta x = \Delta y = \lambda/8, R_c = 25.92$.

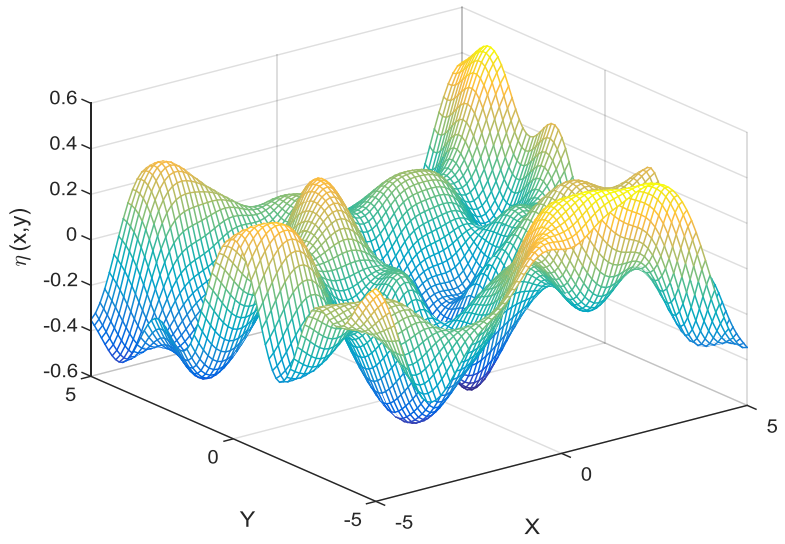

Figure 2.3: Random rough surface showes σ_h, R_c, σ_s

2.2 Electromagnetic roughness and Rayleigh roughness [21],[4]

The first work on the scattering of waves from rough surfaces was made by Lord Rayleigh [21], who considered the problem of a HPPW propagating upon a sinusoidal surface at normal incidence.

This work led to the so-called Rayleigh roughness criterion, which makes it possible to establish the degree of EM roughness of a rough surface. It is used in practice in several simple models to describe the EM wave scattering from random rough surfaces. For instance, in ocean remote sensing, it is used to calculate the grazing incidence forward radar propagation over sea surfaces; in optics to determine optical constants of films model. The roughness (from

an EM point of view) of a surface depends obviously on its height variations, but it is also related to the incident wavelength. Indeed, the EM roughness of a surface is related to the phase variations $\delta_{\phi r}$ of the wave reflected by the surface, owing to the surface height variations.

It is obtained under the Kirchhoff-tangent plane approximation, which is valid for large surface curvature radii and small slopes.

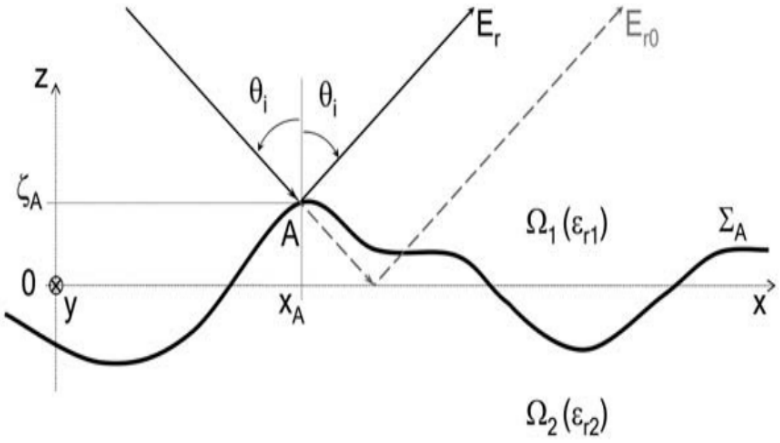

Figure 2.4: Electromagnetic roughness (in reflection) of a random rough surface: phase variations of the reflected wave owing to the surface roughness

Let us consider an incident plane wave inside a medium 1 of wavenumber k_1 on a rough surface with angle θ_i as in Figure 2.3. For the case of a random rough surface considered here, the total reflected field E_r results from the contribution of all reflected fields from the random heights of the rough surface. Then, to quantify the EM surface roughness, it is the phase variation $\delta_{\phi r}$ of the reflected field around its mean value (which corresponds to the phase of the mean plane surface) that must be considered. For the

case of a rough surface (see Figure 2.4), the phase variation $\delta_{\phi r}$ is given by the relation [2]:

$$\delta_{\phi r} = 2k_1\delta_{\eta A}\cos\theta_i \tag{2.12}$$

Where $\delta_{\eta A}$=$\eta_A - \langle\eta_A\rangle$ is the height variation, and θ_i is the incidence angle, $\langle\eta_A\rangle$ is the mean value of the rough surface heights (with $\langle\cdots\rangle$ representing the statistical average), which is equal to 0. If the phase variation is negligible, $\delta_\phi \ll \pi$, for all positions of these points on the surface, then all the waves scattered (reflected) by the random rough surface are nearly in phase and will consequently interfere constructively. The surface is then considered as slightly or very slightly rough: it may be assimilated to a flat surface.

On the contrary, if the phase variation checks $\delta_\phi \sim \pi$, these rays interfere destructively. The contribution of the energy scattered in this specular direction is then weak, and the surface is then considered as rough. The Rayleigh roughness criterion [21] assumes the following condition: if $\delta_\phi < \frac{\pi}{2}$, the waves interfere constructively. Consequently, the surface can be considered as very slightly rough or even flat if $\delta_\phi \ll \frac{\pi}{2}$. Conversely, if $\delta_\phi > \frac{\pi}{2}$, the waves interfere destructively, and the surface can be considered as rough. To apply this local approach to the whole surface, it is necessary to consider a mean phenomenon, which implies quantifying this phenomenon by a statistical average on δ_ϕ.

The mean value of the surface heights being taken as zero, $\langle\eta_A\rangle = 0$, the Rayleigh roughness parameter is quantified by the variance of the phase vari-

ation $\sigma^2_{\delta\phi}$. Knowing that $\langle \eta_A^2 \rangle = \sigma_h^2$ and $\langle \delta_\phi \rangle = 0$, it is defind by:

$$\sigma^2_{\delta\phi} = \langle (\delta_\phi)^2 \rangle = \langle (2k_1 \delta_{\eta_A} \cos\theta_i)^2 \rangle = 4k_1^2 \sigma_h^2 cos^2\theta_i \tag{2.13}$$

The Rayleigh roughness parameter is then defined from the RMS value σ_{δ_ϕ}. Its definition varies by a factor (coefficient) of 2, depending on the authors; here we take:

$$R_a = k_1 \sigma_h cos\theta_i, \tag{2.14}$$

which corresponds to $R_a = \frac{\sigma_{\delta_\phi}}{2}$. The Rayleigh roughness criterion is then:

$$R_a < \frac{\pi}{4} \tag{2.15}$$

which corresponds to $\sigma_h \cos\theta_i < \lambda/8$, it depends on the incident wavelength $\lambda_1 \equiv \lambda$. It is the ratio σ_η/λ that determines the degree of roughness of a surface, for a given incidence angle. Besides, the influence of the term $\cos\theta_i$ is nearly always neglected. Nevertheless, it is not negligible when the incidence angle becomes grazing, $\theta_i \to 90°$: this implies that a surface can be considered as rough for moderate incidence angles and becomes only slightly rough for grazing angles.

If we look more closely at this roughness criterion, we can see that equation (2.15) can be rewritten in the form:

$$\sigma_h < \frac{1}{8} \frac{\lambda_1}{\cos\theta_i} = \frac{1}{8} \lambda_{app} \tag{2.16}$$

where $\lambda_{app} = \lambda_1 / \cos\theta_i$ can be defined as an apparent wavelength along the normal to the mean surface.

In the next section we will explain Kirchhoff Approximation (KA) and adopt a mathmeatical model, to calculate RCS of a flat (plate) surface and a very rough surface and check the validity domain of this approximation by comparing the result with MLFMM method.

2.3 Presentation of the model: KA for 3D problem

Physical optics or Kirchhoff Approximation (also referred to as the tangent plane approximation) is a asymptotic method based on the simplification of Stratton-Chu integral equations in which the currents on the surface are approximated by the tangential field of the geometrical optics [6]. PO does not take into account creeping waves or discontinuities of the surface. This limits the area of validity of the PO to regions close to the specular directions and forward scattering [23].

The PO is nevertheless very interesting because it lies in a simple integration, which can be performed analytically without much difficulty on flat surfaces (square or triangular meshes for example); any object can be processed by the method via a mesh in elementary plane surfaces. Equation (1.42) can be written according to currents as [7]:

$$\mathbf{E}_{sr}(\mathbf{R}') = \int\int_S [G(\mathbf{R},\mathbf{R}')i\omega\mu\mathbf{J}_s(\mathbf{R}) + \mathbf{M}_s(\mathbf{R}) \times \nabla G(\mathbf{R},\mathbf{R}') + \frac{i}{\omega\mu}[\mathbf{J}_s.\nabla]\nabla G(\mathbf{R},\mathbf{R}')]ds. \tag{2.17}$$

Where $\mathbf{J}_s = \hat{\mathbf{n}} \times \mathbf{H}(\mathbf{R})$ is the surface electrical current and $\mathbf{M}_s = -\hat{\mathbf{n}} \times \mathbf{E}(\mathbf{R})$ the surface magnetic current. After some developments by taking the curl of green's function and use equation (1.42), we obtain a new expression of the electric field scattered by an obstacle :

$$\mathbf{E}_{sr}(\mathbf{R}) = \int\int_S [(1 + ikr - k^2r^2)\mathbf{J}_s(\mathbf{R}) + \frac{ikr - k^2r^2}{Z}\mathbf{M}_s(\mathbf{R}) \times \hat{\mathbf{r}} + (-3 - 3ikr + k^2r^2)(\hat{\mathbf{r}}.\mathbf{J}_s(\mathbf{R}))\hat{\mathbf{r}}]\frac{G(\mathbf{R},\mathbf{R}')}{r^2}ds. \tag{2.18}$$

where $G(\mathbf{R},\mathbf{R}') = \frac{e^{ikr}}{4\pi r}$, and $r = |\mathbf{R} - \mathbf{R}'|$, represent green's function in free space for 3-D scattering; Z and k denote the impedance and wavenumber of the propagation medium. Equation (2.18) is a general equation that can be used in near and far fields. The goal of the PO approximation is to solve the integral equation by using simplifying assumptions:

- High frequency hypothesis: the dimensions of the object are much higher than the wave length. The current densities on the surface of the object decrease very rapidly and can be considered null in the shadowing zone. The PO method does not take into account counts creeping waves, nor discontinuities.

- The radii curvature of the illuminated surface is much greater than the

wavelength. The approximation of the PO is also called approximation of the tangent plane: where the surface linked to an infinite plane at each of its points. This infinite plane corresponds to the plane tangent to the surface at the point considered. The surface is then qualified as locally flat. Under this hypothesis, the field reflected by the surface can be express very simply by applying laws of Snell-Descart. The Fresnel coefficient allows knowing its amplitude, and the law of Snell-Descartes gives the direction.

In the case of Perfectly Conductive surface (PC) all incident field are reflected, then: $\mathbf{H}_{sr}(\mathbf{R}) = \mathbf{H}_i(\mathbf{R})$ and $\mathbf{E}_{sr}(\mathbf{R}) = -\mathbf{E}_i(\mathbf{R})$, where $\mathbf{E}_i$, $\mathbf{H}_i$ are the EM incident fields respectively. So we can then express the surface current densities in term of incident fields as:

$$\mathbf{J}_s(\mathbf{R}) = \hat{\mathbf{n}} \times (\mathbf{H}_i(\mathbf{R}) + \mathbf{H}_{sr}(\mathbf{R})) = 2(\hat{\mathbf{n}} \times \mathbf{H}_i(\mathbf{R})), \tag{2.19}$$

and

$$\mathbf{M}_s(\mathbf{R}) = \hat{\mathbf{n}} \times (\mathbf{E}_i(\mathbf{R}) + \mathbf{E}_{sr}(\mathbf{R})) = 0, \tag{2.20}$$

Then for Perfect Conductors (PC) equation (2.18) becomes:

$$\begin{aligned}\mathbf{E}_{sr} = \int\int_S [(1 + ikr - k^2r^2)(\hat{\mathbf{n}} \times (\mathbf{H}_i(\mathbf{R}) + (-3 - 3ikr + k^2r^2) \\ (\hat{\mathbf{r}}.(\hat{\mathbf{n}} \times \mathbf{H}_i(\mathbf{R}))\hat{\mathbf{r}}] \frac{G(\mathbf{R}, \mathbf{R}')}{r^2} ds.\end{aligned} \tag{2.21}$$

2.4 Formulation for a PC scatterer in far field

The problem can be simplified by applying the far field condition. If the surface element ds is away from the observation point such as $k_0 r >> 1$ then the terms $\frac{1}{r}$ and $\frac{1}{r^2}$ in equation (2.21) can be considered null. Furthermore we consider that the surface is placed in a medium assimilated to the vacuum with geometry shown in Figure 2.4. Then we obtain a simplified expression of the equation (2.21):

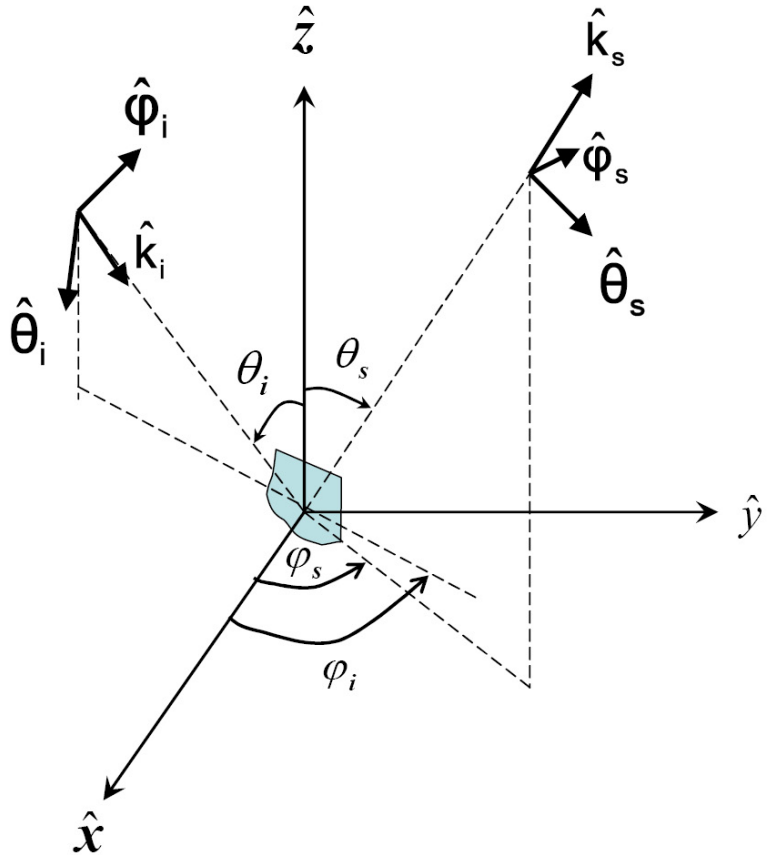

Figure 2.5: illustration of the polarization bases used in transmission and reception

$$\mathbf{E}_{sr}(\mathbf{R}') = \frac{i\omega\mu}{4\pi R'} e^{ik_0 R'} \int\int_S [\mathbf{J}_s(\mathbf{R}) + (\hat{\mathbf{r}}.\mathbf{J}_s(\mathbf{R}))\hat{\mathbf{r}}] e^{-ik_0 \hat{\mathbf{k}}_s} ds. \qquad (2.22)$$

Under the condition of a plane wave illumination in the direction $\hat{\mathbf{k}}_i$, the incident electric field can be described in spherical coordinates, as follows:

$$\mathbf{E}_i(\mathbf{R}) = \mathbf{E}_i e^{ik_0\hat{\mathbf{k}}_i.\mathbf{R}} = (E_i^{\theta}\hat{\boldsymbol{\theta}}_{\boldsymbol{i}} + E_i^{\phi}\hat{\boldsymbol{\phi}}_{\boldsymbol{i}})e^{ik_0\hat{\mathbf{k}}_i.\mathbf{R}}, \tag{2.23}$$

and then magnetic field is:

$$\mathbf{H}_i(\mathbf{R}) = \frac{1}{Z_0}\hat{\mathbf{k}}_i \times \mathbf{E}_i(\mathbf{R}). \tag{2.24}$$

Expressing the different vectors as shown in Figure 2.5, in the Cartesian coordinates we get,

$$\hat{\mathbf{k}}_i = \begin{bmatrix} \sin\theta_i \cos\phi_i \\ \sin\theta_i \sin\phi_i \\ -\cos\theta_i \end{bmatrix} \tag{2.25}$$

and

$$\hat{\mathbf{k}}_s = \begin{bmatrix} \sin\theta_s \cos\phi_s \\ \sin\theta_s \sin\phi_s \\ \cos\theta_s \end{bmatrix} \tag{2.26}$$

The vector $\mathbf{H}_i$ can be written in cartsian coordinates ($\hat{\mathbf{x}}$, $\hat{\mathbf{y}}$,$\hat{\mathbf{z}}$), as follows where we get the matrix form for each components according to spherical components E_i^{θ} and E_i^{ϕ},

$$\begin{bmatrix} H_{ix} \\ H_{iy} \\ H_{iz} \end{bmatrix} = \frac{1}{Z_0} \begin{bmatrix} E_i^{\phi} \cos(\theta_i) \cos(\phi_i) - E_i^{\theta} \sin(\phi_i) \\ E_i^{\phi} \cos(\theta_i) \sin(\phi_i) + E_i^{\theta} \cos(\phi_i) \\ E_i^{\phi} \sin(\theta_i) \end{bmatrix} e^{ik_0 \hat{\mathbf{k}}_i . \mathbf{R}} \tag{2.27}$$

and the normal to the surface $\hat{\mathbf{n}}(\mathbf{R})$ expressed by [7]:

$$\hat{\mathbf{n}}(\mathbf{R}) = n_x \hat{\mathbf{x}} + n_y \hat{\mathbf{y}} + n_z \hat{\mathbf{z}} = \frac{-z_x \hat{\mathbf{x}} - z_y \hat{\mathbf{y}} + \hat{\mathbf{z}}}{\sqrt{1 + z_x^2 + z_y^2}}, \tag{2.28}$$

where $z_x = \frac{\partial z}{\partial x}$ is the slope along the x-axis, and $z_y = \frac{\partial z}{\partial y}$ is the slope along y-axis. Using the PO approximation, $\mathbf{J}_s(\mathbf{R}) = 2\hat{\mathbf{n}}(\mathbf{R}) \times \mathbf{H}_i(\mathbf{R})$, the components of surface current are given from the equations (2.25), (2.27) and (2.28)

$$\mathbf{J}_s = \frac{2}{Z_0} \begin{bmatrix} E_i^{\phi}(n_y \sin\theta_i - n_z \cos\theta_i \sin\phi_i) - E_i^{\theta}(n_z \cos\phi_i) \\ -E_i^{\phi}(n_z \cos\theta_i \cos\phi_i + n_x \sin\theta_i) + E_i^{\theta}(n_z \sin\phi_i) \\ E_i^{\phi}(n_x \cos\theta_i \sin\phi_i - n_y \cos\theta_i \cos\phi_i) + E_i^{\theta}(n_x \cos\phi_i + n_y \sin\phi_i) \end{bmatrix} e^{ik_0 \hat{\mathbf{k}} . \mathbf{R}} \tag{2.29}$$

and we can write $\mathbf{J}_s$ as:

$$\mathbf{J}_s = \bar{\mathbf{J}}_s \begin{bmatrix} E_i^{\theta} \\ E_i^{\phi} \end{bmatrix} \tag{2.30}$$

or

$$\bar{\mathbf{J}}_s = \frac{2}{Z_0} \begin{bmatrix} J_x^{\theta} & J_x^{\phi} \\ J_y^{\theta} & J_y^{\phi} \\ J_z^{\theta} & J_z^{\phi} \end{bmatrix} e^{ik_0 \hat{\mathbf{k}} . \mathbf{R}} \tag{2.31}$$

from equation (2.29) we have:

$$\bar{\mathbf{J}}_s = \frac{2}{Z_0}\begin{bmatrix} -n_z\cos\phi_i & n_y\sin\theta_i - n_z\cos\theta_i\sin\phi_i \\ n_z\sin\phi_i & -(n_z\cos\theta_i\cos\phi_i + n_x\sin\theta_i) \\ n_x\cos\phi_i + n_y\sin\phi_i & n_x\cos\theta_i\sin\phi_i - n_y\cos\theta_i\cos\phi_i \end{bmatrix} e^{ik_0\hat{\mathbf{k}}_i.\mathbf{R}} \tag{2.32}$$

From equations (2.22) and (2.32) we can write:

$$\mathbf{E}_{sr}(\boldsymbol{R'}) = \frac{i\omega\mu}{2\pi R' Z_0} e^{ik_0 R'} \bar{\mathbf{D}}_s \begin{bmatrix} E_i^\theta \\ E_i^\phi \end{bmatrix} \tag{2.33}$$

where $\bar{\mathbf{D}}_s$ matrix is defined the following :

$$\bar{\mathbf{D}}_s = \begin{bmatrix} S_{11} & S_{12} & S_{13} \\ S_{21} & S_{22} & S_{23} \\ S_{31} & S_{32} & S_{33} \end{bmatrix} \begin{bmatrix} I_{11} & I_{12} \\ I_{21} & I_{22} \\ I_{31} & I_{32} \end{bmatrix} \tag{2.34}$$

with

$$I_{11} = \int\int_s J_x^\theta . e^{ik_0(\hat{\mathbf{k}}_i - \hat{\mathbf{k}}_s).\mathbf{R}} ds, \tag{2.35}$$

$$I_{12} = \int\int_s J_x^\phi . e^{ik_0(\hat{\mathbf{k}}_i - \hat{\mathbf{k}}_s).\mathbf{R}} ds, \tag{2.36}$$

$$I_{21} = \int\int_s J_y^\theta . e^{ik_0(\hat{\mathbf{k}}_i - \hat{\mathbf{k}}_s).\mathbf{R}} ds, \tag{2.37}$$

$$I_{22} = \int\int_s J_y^\phi . e^{ik_0(\hat{\mathbf{k}}_i - \hat{\mathbf{k}}_s).\mathbf{R}} ds, \tag{2.38}$$

$$I_{31} = \int\int_s J_z^\theta . e^{ik_0(\hat{\mathbf{k}}_i - \hat{\mathbf{k}}_s).\mathbf{R}} ds, \tag{2.39}$$

$$I_{13} = \int\int_s J_z^\phi . e^{ik_0(\hat{\mathbf{k}}_i - \hat{\mathbf{k}}_s).\mathbf{R}} ds, \tag{2.40}$$

and

$$\begin{cases} S_{11} = -\sin^2\theta_s \sin^2\phi_s - \cos^2\theta_s, \\ S_{12} = \sin^2\theta_s \sin\phi_s \cos\phi_s, \\ S_{13} = \sin\theta_s \cos\theta_s \cos\phi_s \\ S_{22} = -\sin_s^{\theta} \cos^2\phi_s - \cos^2\theta_s, \\ S_{23} = \sin\theta_s \cos\theta_s \sin\phi_s, \\ S_{33} = -\sin^2\theta_s, \end{cases} \tag{2.41}$$

Thus we obtain the components of scattered field in $(\hat{\mathbf{x}}, \hat{\mathbf{y}}, \hat{\mathbf{z}})$:

$$\begin{bmatrix} E_{sr}^x \\ E_{sr}^y \\ E_{sr}^z \end{bmatrix} = P\bar{\mathbf{D}}_s \begin{bmatrix} E_i^{\theta} \\ E_i^{\phi} \end{bmatrix}, \tag{2.42}$$

where $P{=}\frac{i\omega\mu}{2\pi R'\eta_0} e^{ik_0R'}$ is a scalar that depends on the observation distance, the frequency, and EM properties of the incident medium. The components of the scattered field in the Cartesian coordinate system are expressed according to spherical componenets using the spherical rotation matrix ($\bar{\mathbf{R}}_s$) as follows:

$$\bar{\mathbf{R}}_s = \begin{bmatrix} \sin\theta_s\cos\phi_s & \cos\theta_s\cos\phi_s & -\sin\phi_s \\ \sin\theta_s\sin\phi_s & \cos\theta_s\sin\phi_s & \cos\phi_s \\ \cos\theta_s & -\sin\theta_s & 0 \end{bmatrix} \tag{2.43}$$

$$\begin{bmatrix} E_{sr}^{\theta} \\ E_{sr}^{\phi} \end{bmatrix} = P\bar{\mathbf{R}}_s{}^T\bar{\mathbf{D}}_s \begin{bmatrix} E_i^{\theta} \\ E_i^{\phi} \end{bmatrix} \tag{2.44}$$

Finally, the components of the incident and scattered field are linked by the next expression:

$$\mathbf{E}_{sr} = \bar{\mathbf{S}}\mathbf{E}_i \tag{2.45}$$

where $\bar{\mathbf{S}} = P\bar{\mathbf{R}}_s^T\bar{\mathbf{D}}_s$ is the scattering matrix.

$$\bar{\mathbf{S}} = \begin{bmatrix} S_{\theta\theta} & S_{\theta\phi} \\ S_{\phi\theta} & S_{\phi\phi} \end{bmatrix} \tag{2.46}$$

Then we finally obtain RCS matrix :

$$\bar{\boldsymbol{\sigma}} = 4\pi R'^2 \begin{bmatrix} |S_{\theta\theta}|^2 & |S_{\theta\phi}|^2 \\ |S_{\phi\theta}|^2 & |S_{\phi\phi}|^2 \end{bmatrix} \tag{2.47}$$

The previous equations can be defined as the numerical representation of the KA or PO model, we will apply this model for the case of a PC plate, then the case of PC rough surface will be tested.

2.4.1 KA to study the scattering from a plate

After we introduced the Kirchhoff Approximation (KA) for 3D rough surface we start to check the validation of KA by testing it with a simple case of zero height which is a smooth surface (plate). Consider a plate of surface $S = L_x \times L_y$ located in the plane $(\hat{\mathbf{x}}, O, \hat{\mathbf{y}})$, as shown in Figure 2.6.

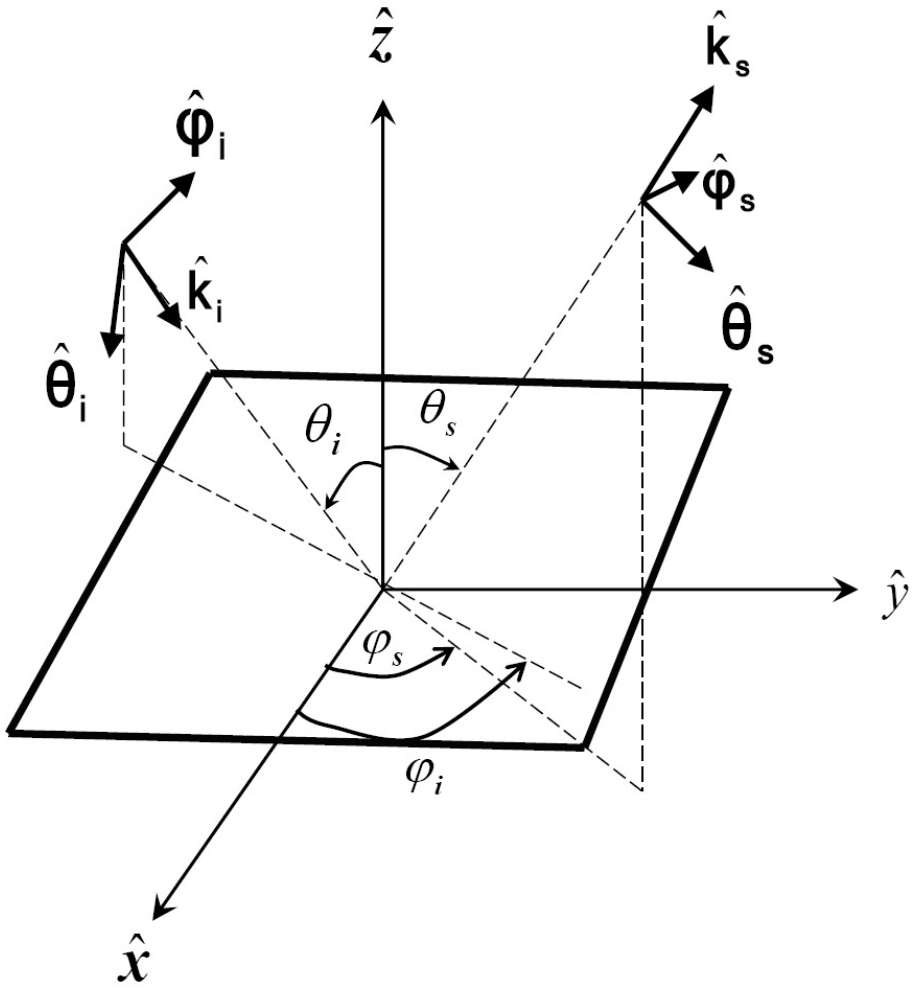

Figure 2.6: Geometry of the problem: illustration of the smooth plate.

The normal to the surface is directed along the z-axis, the method of the PO is always compared to the reference models from FEKO software.

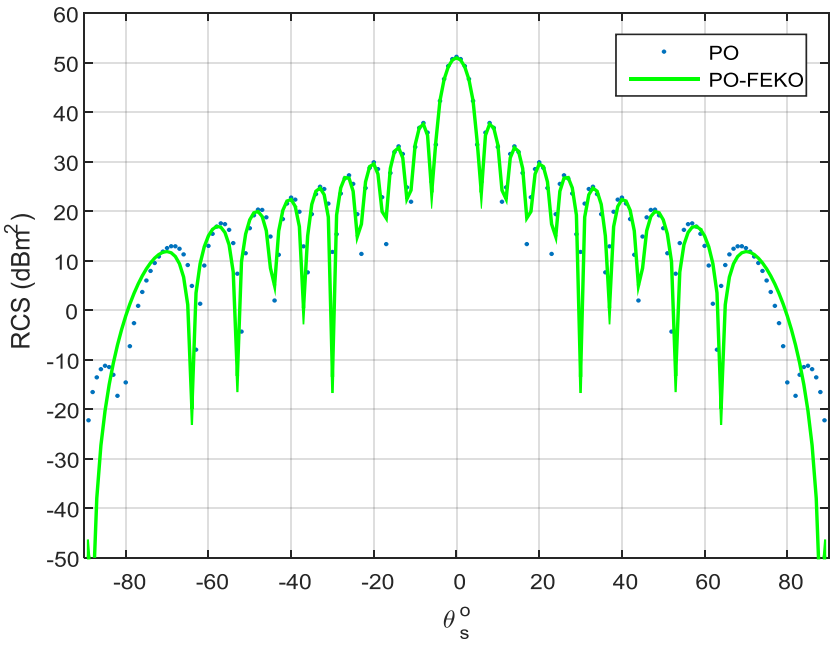

Figure 2.7: Comparison of the bistatic RCS of the scattered field of a plate, obtained with the PO-FEKO and the proposed method PO, with HH referto $\theta\theta$ polarization, $L_{cx} = L_{cy} = 1.2\lambda_0, \triangle x = \triangle y = \lambda_0/8, \theta_i = \varphi_i = 0^o$.

We noticed from Figure 2.7 that the proposed model KA is a good approximation over all range of scattering angles $\theta_s \in [-90°; +90°]$.

After that we will check the validity of our approximation when incident angle θ_i is changed, using the same specifications, $L_{cx} = L_{cy} = 1.2$, $\lambda_0 = 1m$, $\triangle x = \triangle y = \lambda_0/8$, $\varphi_i = 0^o$, and $\theta_i = 60^o$.

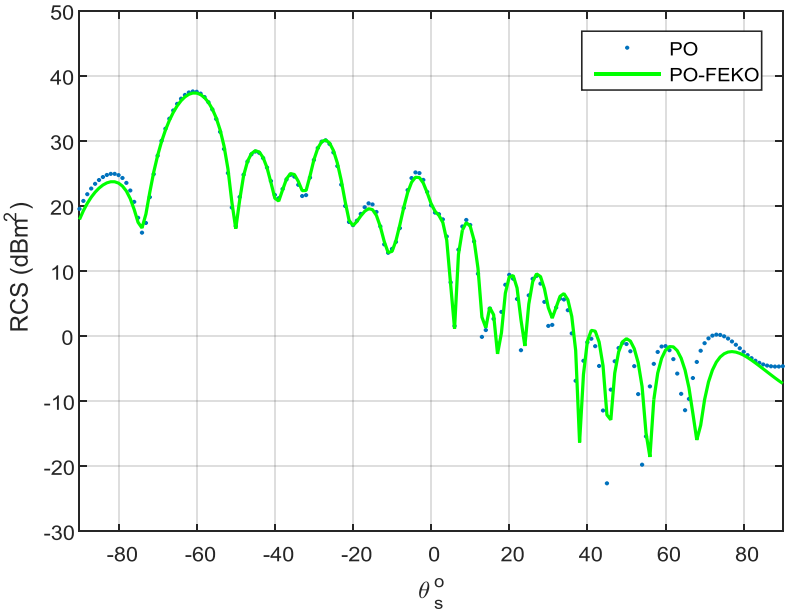

Figure 2.8: Comparison of the bistatic RCS of the scattered field of the plate, obtained with PO-FEKO and the proposed method PO, with HH polarization, $L_{cx} = L_{cy} = 10\lambda_0$,$\triangle x = \triangle y = \lambda_0/8$, $\theta_i = 60, \varphi_i = 0^o$.

We notice that the maximum power is in the direction of the incident angle θ_i as illustrated in Figure 2.8 and PO still a good approximation. Finally, as shown in Figure 2.9 the RCS is plotted according to the observation angles for both MLFMM-FEKO and our proposed approximation PO. The plate is of $L_{cx} = L_{cy} = 1.2$, $\lambda_0 = 1m$, the sampling steps of the surface are $\triangle x = \triangle y = \lambda_0/8$, $\varphi_i = 0^o$, and $\theta_i = 0^o$ (normal incidence).

We notice that the PO method is in a good agreement with the MLFMM around the specular direction $\theta_s = 0$. Other values of θ_i, between -90^o and 90^o have produced the same conclusion of obtaining maximum power for $\theta_i = \theta_s$: the specular direction.

We also observe that the PO method does not allow to evaluating correctly the RCS for grazing viewing angles, this being mainly due the concentra-

tion of currents on the edge causing edge diffraction that are not taken into account in the PO.

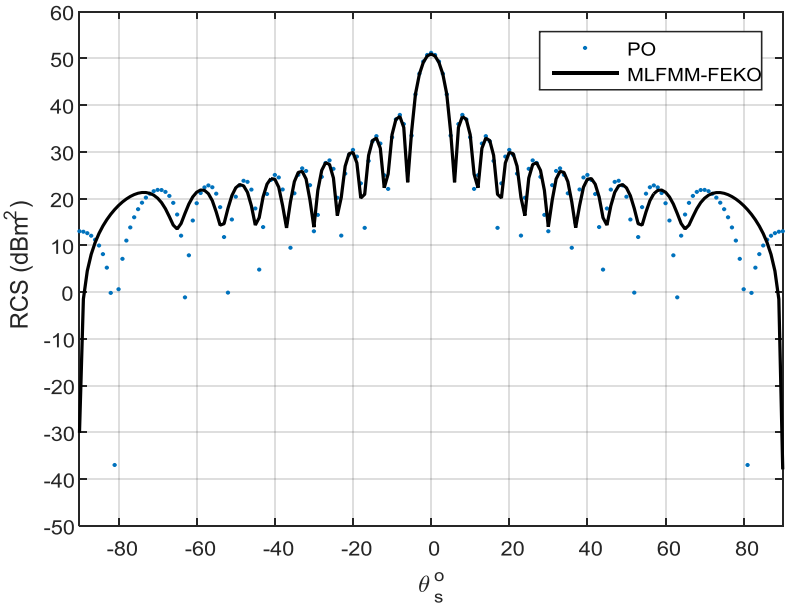

Figure 2.9: Comparison of the bistatic RCS and phase of the scattered field of the plate, obtained with the MLFMM and the proposed method PO, with VV polarization, $L_x = L_y = 12\lambda_0, \triangle x = \triangle y = \lambda_0/8, \theta_i = \varphi_i = 0^o$.

So the total power are in the direction of incident angle and the next Figure 2.10 gets from FEKO simulator shows 3D RCS scattering from plate and current distribution when we take the result from PO-FEKO, we also notice that the current is equally distributed and equal in magnitude.

Figure 2.11. Shows the distribution of current on a plate when using MLFMM for scattering solution in EM simulator. We observe that the currents are not equal on the geometry of the surface, since the MLFMM calculate the effect of current in each part to other parts.

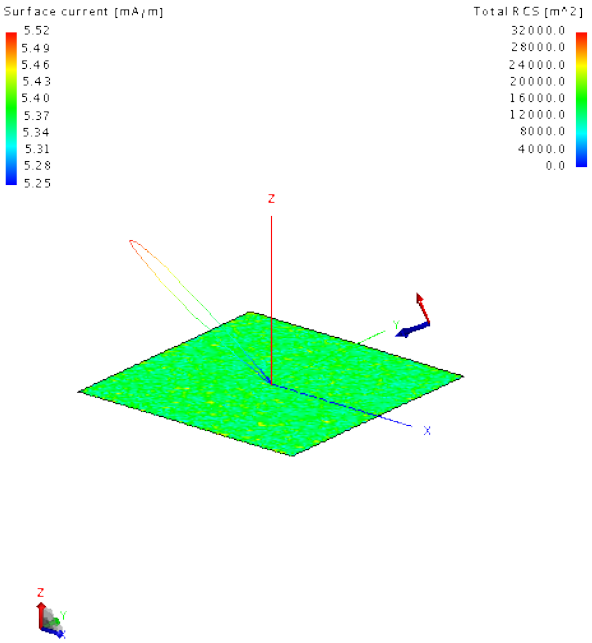

Figure 2.10: Geometry of the problem: illustration of the plate shows the power scattered and the major beam direction calculated using PO

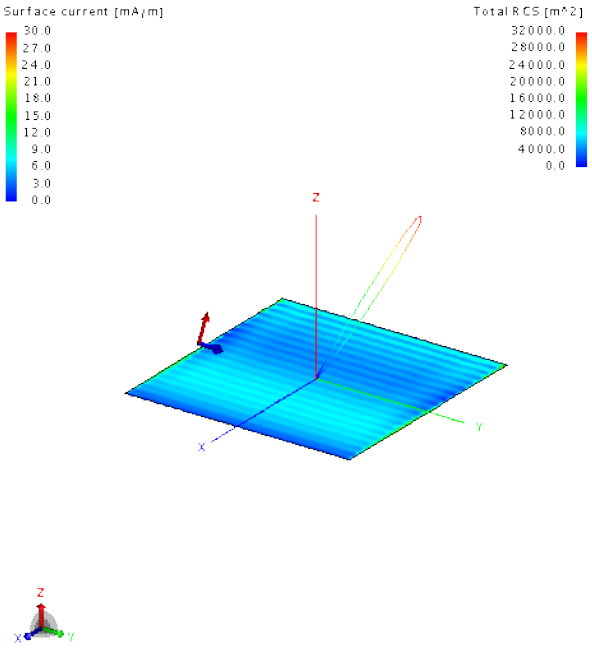

Figure 2.11: Geometry of the problem: illustration of the plate show the current distribution and the major beam direction calculated using MLFMM

2.4.2 KA to study the scattering from two dimensional rough surface (3D problem)

In this section, we will discuss the validity of KA for 3D rough surface and compare the result firstly with FEKO-PO and then with rigorous model MLFMM.

Consider a rough surface of dimension $10\lambda \times 10\lambda$ as shown in Figure 2.12, generated by Gaussian random process, of which autocorrelation function of height is given by $C_h(x,y) = \sigma_h^2 \exp(-x^2/L_{cx}^2 - y^2/L_{cy}^2)$, the correlation lengths $L_{cx} = L_{cy} = 1.2\lambda_0$, and with standard deviation of the heights $\sigma_h = 0.2\lambda_0$, $(\sigma_s = \sqrt{2} \times \sigma_h/L_c \approx 0.24\lambda_0)$.

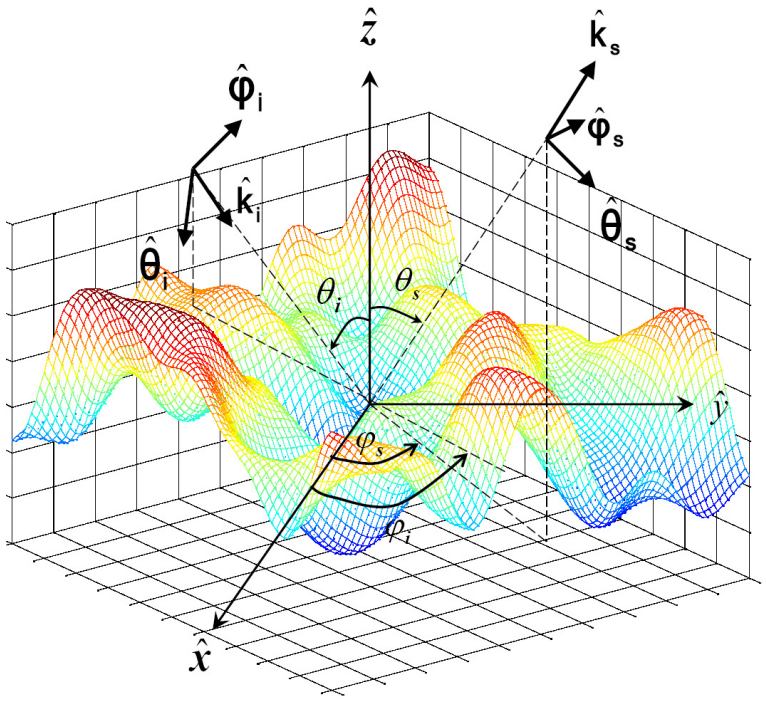

Figure 2.12: Geometry of the problem: illustration of the rough surface

The surface is illuminated by a plane wave in normal incident, $\theta_i = 0^o$, $\varphi_i = 0^o$, the discretizing steps of the surface are $\Delta_x = \Delta_y = \lambda_0/8$. The PO is compared to FEKO-OP in Figure 2.13 and Figure 2.14, on which the RCS

is plotted according to the angle of observation θ_s for both co-polarizations HH.

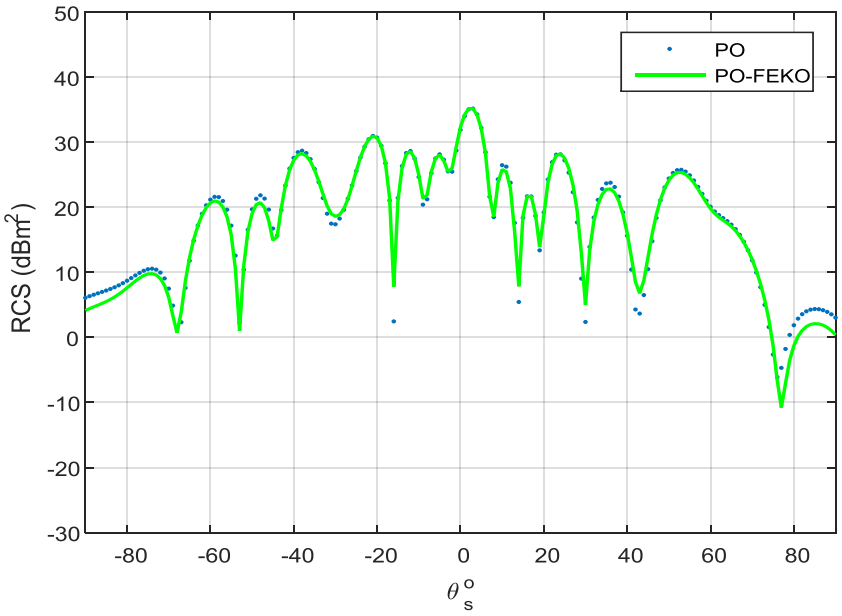

Figure 2.13: Comparison of bistatic RCS obtained with FEKO-PO and proposed PO for HH co-polarization, case of a rough surface of dimension $10\lambda \times 10\lambda$, $\triangle x = \triangle y = \lambda_0/8$, $\theta_i = \varphi_i = 0^o$, $L_{cx} = L_{cy} = 1.2, \sigma_h = 0.2\lambda$

We observe from Figure 2.13 and Figure 2.14 that the result obtained by the proposed PO are in good agreement with those get from FEKO, that means that PO still a good approximation.

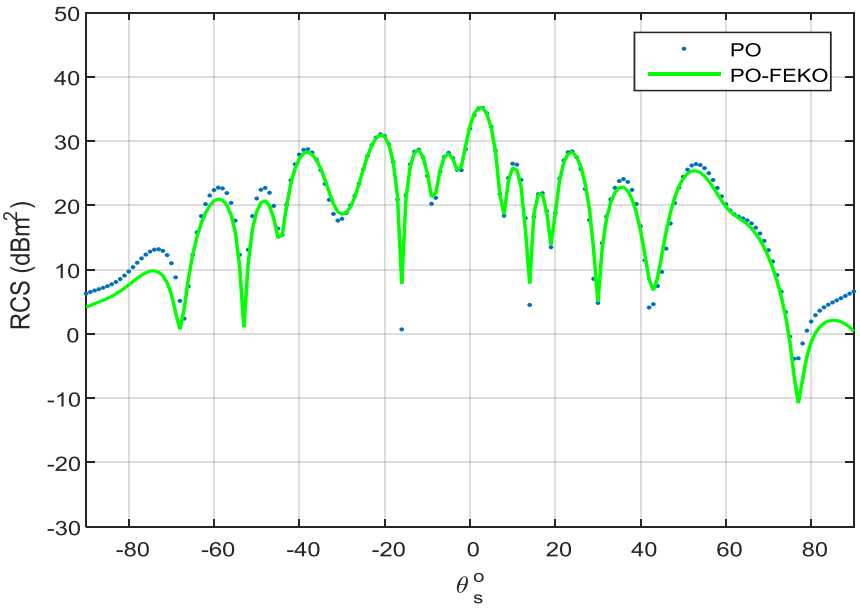

Figure 2.14: Comparison of bistatic RCS obtained with FEKO-PO and proposed PO for VV co-polarization, case of a rough surface of dimension $10\lambda \times 10\lambda$, $\triangle x = \triangle y = \lambda_0/8$, $\theta_i = \varphi_i = 0^o$, $L_{cx} = L_{cy} = 1.2, \sigma_h = 0.2\lambda$

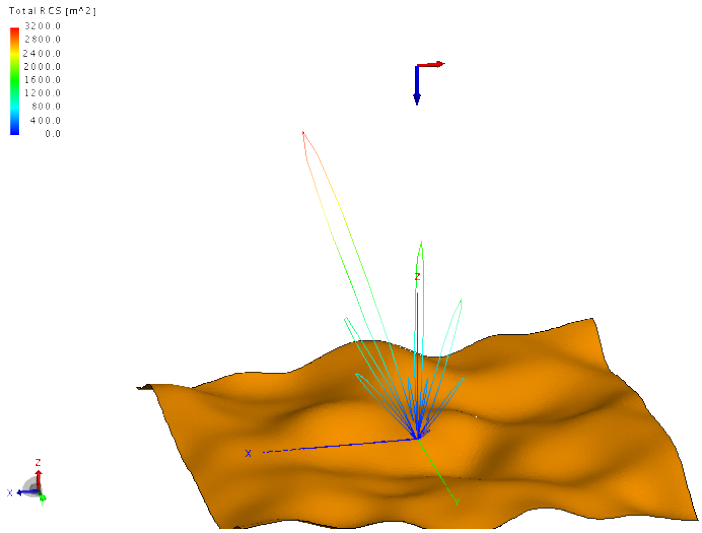

Figure 2.15: Geometry of the problem: illustration of the rough surface showing the power scattered and the major beam direction

From Figure 2.15 we notice that maximum power is located around the specular direction. Since the surface is rough, the contribution of the specular component decreases as the scattered power in the other directions increases. Figure 2.14 which shows the 3D power scattered from geometry obtained by

EM simulator calculated by MLFMM method.

Another comparison of the results of FEKO-PO, will be then done with FEKO-MLFMM using the same specification $\sigma_h = 0.2$, dimension $10\lambda \times 10\lambda, L_{cx} = L_{cy} = 1.2$, as in Figure 2.16.

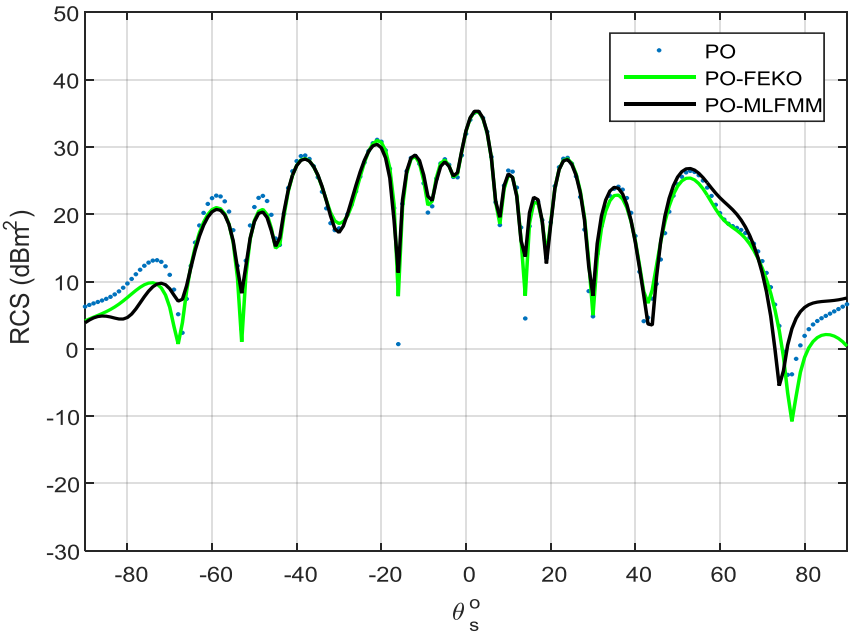

Figure 2.16: Comparison of bistatic RCS obtained with FEKO-MLFMM and proposed PO for HH co-polarization, case of a rough surface of dimension $10\lambda \times 10\lambda$, $\triangle x = \triangle y = \lambda_0/8$, $\theta_i = \varphi_i = 0^o$, $L_{cx} = L_{cy} = 1.2$, $\sigma_h = 0.2\lambda$

As seen from Figure 2.16, we also observe that PO approximation is in agreement with the MLFMM for most scattering angles θ_s, except for grazing angles.

After we checked the validity domain of PO from smooth to very rough surface and compare the results with FEKO. We will introduce the shadowing function and show how to insert this correction function into KA in the last chapter.

Chapter 3

Electromagnetic Scattering from Two Dimensional Rough Surfaces using iterative method with shadowing effect

---

In this chapter, the scattering field intensities of random rough surface are derived by inserting a correction factor called illumination function or shadowing function, to improve the asymptotic KA model described in the previous chapter. And then we will check the validity of this new approximation and compare the results with FEKO-MLFMM.

After we introduce and discuss the shadowing function, we present a new approaches called Iterative Physical Optics (IPO) which focuses in studying the effect of current between each part in the geometry and how this effect react to improve and correct our mathematical assumption of PO.

From the previous chapter, the expressions of the field scattered in the far-field zone of the surface make it possible to calculate the scattered intensities through the so-called scattering coefficient (in reflection and transmission), our mathematical model is checked for the validation. Now, in order to improve KA we will introduce the shadowing function and then combine it with the KA technique.

3.1 Bistatic Shadowing Functions in Reflection

EM scattering from rough surface is affected by surface shadowing when the angle of incidence is large, traditional rough surface scattering theories such as small-perturbation method and KA do not directly include shadowing effects. Attempts have been made to include shadowing in these models by incorporating "a shadowing function"[26]. In this section we will introduce a correction factor to represent the shadowing effect. Firstly, we will introduce monostatic shadowing function and then develop the bistatic shadowing function.

3.1.1 Monostatic Shadowing Functions

There are a number of theories for the scattering by randomly rough surfaces, based on a "ray-optics"approximation, whose validity may be extended by properly accounting for surface shadowing . Wagners and Smiths approaches [27], [28], are used to describe the shadowing function with single reflection for a stationary rough surface.

Their formulation assumes that the surface is one dimensional with a Gaussian process, where the correlation between the surface slopes and heights is neglected. From these works, Bourlier et al [29] have extended the shadowing function for any uncorrelated and correlated Gaussian processes. With a Gaussian process, they showed for an infinite observation length that the Smith results are more accurate than Wagners and the correlation weakly improves the model. The Smith approach is chosen as a starting point to

develop the statistical shadowing function with multiple reflections [30].

The monostatic statistical shadowing function represents the probability that the incidence or scattering beam of direction $\hat{\mathbf{K}}_1$ (and associated angle θ_1) in the medium Ω_1 does not intercept before reaching the surface at the considered point A (of coordinates $\mathbf{R}_A = (x_A, \eta_A)$) as illustrated in Figure 3.1. This probability is conditioned by the surface height and slope at the considered point A and defined for a surface with even statistics [2] as follows:

$$S_1(\mathbf{K}_1 \mid \eta_A, \gamma_A) = \Upsilon(\mu_1 - \gamma_A)[\, P_h(\eta_A) - P_h(-\infty)]^{\,\Lambda(\mu_1)} \tag{3.1}$$

where

$$P_h = \int p_h(\eta) d\eta, \tag{3.2}$$

$$\Lambda(\mu_1) = \frac{1}{\mu_1} \int_{\mu_1}^{+\infty} (\gamma - \mu_1) p_s(\gamma) d\gamma, \quad with \quad \mu_1 = |\cot \theta_1|, \tag{3.3}$$

$$\Upsilon(x) = \begin{cases} 1 & if\, x \geq 0 \\ \\ 0 & otherwise \end{cases}, \tag{3.4}$$

In equation (3.3), θ_1 is the incidence angle (θ_i such that $\theta_i \in [-\pi/2; 0]$ for oriented angles) or the scattering angle ($\theta_s \in [-\pi/2; +\pi/2]$), with $\mu_1 = |\cot\, \theta_1|$ the absolute value of the associated slope. P_h is a primitive of the height PDF p_h, p_s is the slope PDF, and Υ is the Heaviside function. In equation (3.1), the term $[P_h(\eta_A) - P_h(-\infty)]^{\Lambda(\mu_1)}$ makes a restriction on the surface height η_A.

The term $[P_h(\eta_A) - P_h(-\infty)]$ tends to 1 when point A is located at a high altitude $\eta_A (\eta_A \to +\infty)$, and then the shadowing function is maximum, that

is to say, the shadowing effect is weak. Indeed, the higher point A, the lower the probability that an incident or scattered wave in the upper medium Ω_1 crosses before reaching the surface at point A, which is important. Reversely, this term tends to 0 when point A is located at a low altitude $\eta_A(\eta_A \to -\infty)$, and the shadowing function tends to 0 as well, that is to say, the shadowing effect is maximum. Indeed, the lower point A is, the higher the probability that an incident or scattered wave in the upper medium Ω_1 crosses the surface before reaching at point A. This is illustrated in Figure 3.1, in which point A' of lower altitude than that of A is in the shadow of the beam with slope μ_1.

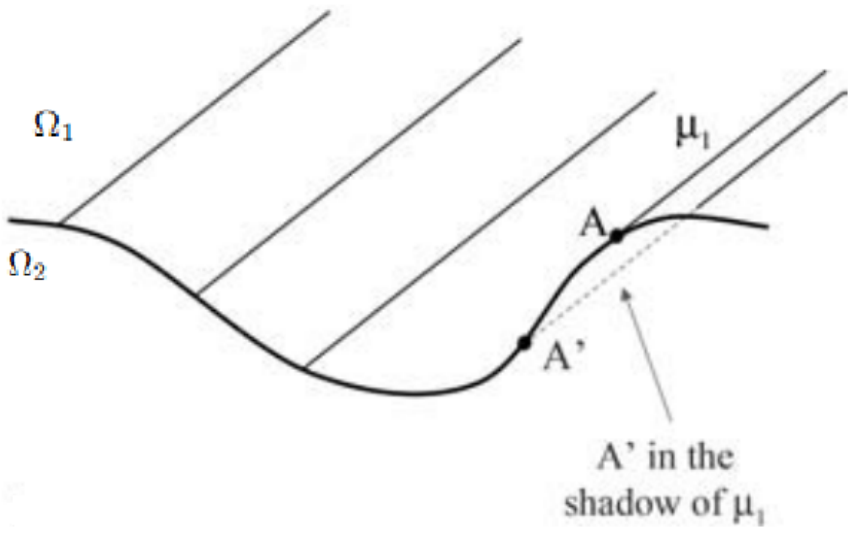

Figure 3.1: Influence of the height of point A

Moreover, the height cumulative distribution function (CDF) $[P_h(\eta_A) - P_h(-\infty)]$ is weighted by the term $\Lambda(\mu_1)$, which takes into account the surface slopes γ that are greater than the absolute slope μ_1 of the wave of direction $\hat{\mathbf{K}}_1$. When $\mu_1 \to 0$ (corresponding to a grazing angle), the function $\Lambda(\mu_1) \to +\infty$, then $S_1 \to 0$ (as $0 \leq P_h(\eta_A) - P_h(-\infty) \leq 1$) : the shadowing effect is maximum.

Reversely, when $\mu_1 \to +\infty$ (corresponding to a zero angle), the function $\Lambda(\mu_1) \to 0$, then $S_1 \to 1$: the shadowing effect is minimum. Thus, this function holds for the fact that for a given surface point A, the lower the absolute slope of the beam of considered wave is, the higher is the shadowing effect.

This is illustrated in Figure 3.2, in which the beam with slope μ_1' that is lower than the beam with slope μ_1 induces a more significant shadowing.

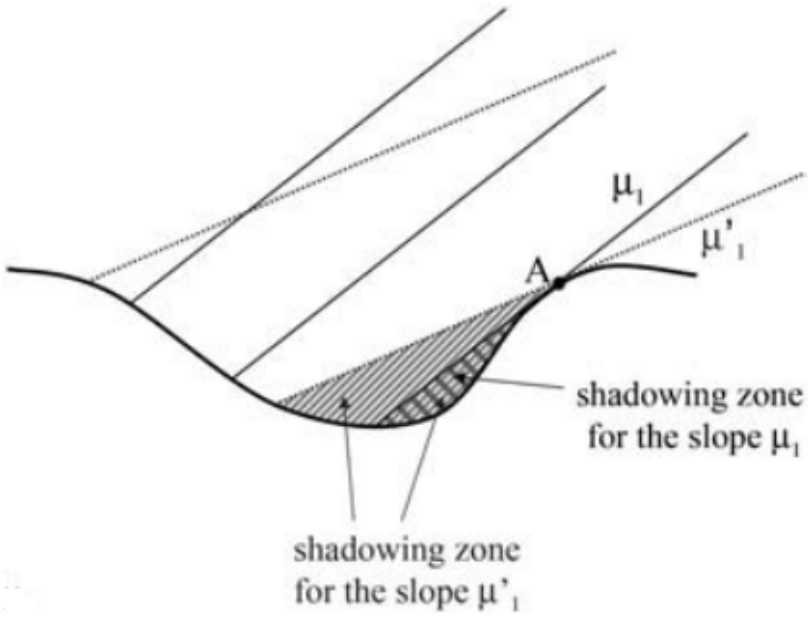

Figure 3.2: The slope of the beam μ_1 on the phenomenon of shadowing (propagation shadowing) of a random rough surface [2]

The term $\Upsilon(\mu_1 - \gamma_A)$ holds for the condition that the absolute value μ_1 of the slope of the incident or scattered wave must be greater than the surface slope γ_A, so that the incident field can contribute to the scattered field. This function then makes a restriction on the surface slope γ_A. This is illustrated in Figure 3.3, in which the beam with slope μ_1' inferior to the surface slope γ_A at point A crosses the surface before reaching it at point A. This point is then in the shadow of the beam with slope $\mu_1' < \gamma_A$. In other words, it is

due to the fact that at a given surface point, owing to the local surface slope at considered point (tangent plane) and to the incidence or scattering angle, the local incidence or scattering angle may be greater than $\pi/2$ in absolute value. This being physically impossible, it is then necessary not to take these points into account.

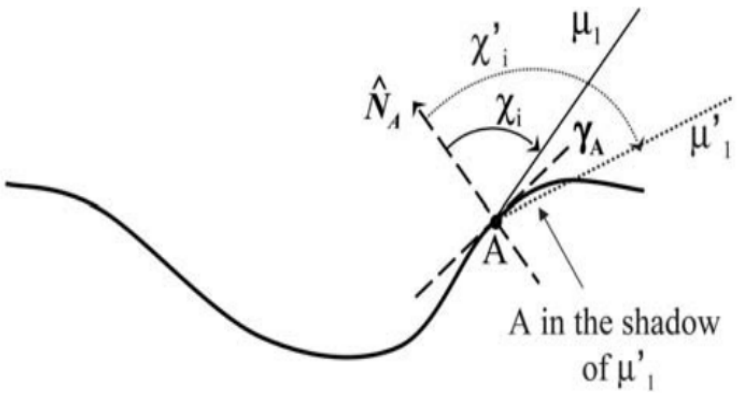

Figure 3.3: Phenomenon of shadowing of a random rough surface [2]

3.1.2 Bistatic Shadowing Functions

The bistatic statistical shadowing function in the case of reflection of a wave in direction $\hat{\mathbf{K}}_i$ by a medium Ω_1 onto a medium Ω_2 in the direction of reflection $\hat{\mathbf{K}}_r$ has been expressed in Wanger [30] and Boulier [29]. For the case of single reflection inside Ω_1, the expression of S_{11} is given in the convention of oriented angles $\theta_i \in [-\pi/2; 0]$, as Figure 3.4 by [2] :

$$S_{11}(\mathbf{K}_i, \mathbf{K}_r \mid \eta_A, \gamma_A) = \begin{cases} S_1(\mathbf{K}_r \mid \eta_A, \gamma_A) & if \quad \theta_r \in [-\pi/2; \theta_i[\\ S_1(\mathbf{K}_i \mid \eta_A, \gamma_A) & if \quad \theta_r \in [\theta_i; 0[\\ S_1(\mathbf{K}_i \mid \eta_A, \gamma_A) S_1(\mathbf{K}_r \mid \eta_A, \gamma_A) & if \quad \theta_r \in [0; +\pi/2[\end{cases} \tag{3.5}$$

where $\mathbf{K}_{i,r}$ are the incident and reflected wave vectors, with $\mu_{i,r} = \mid \cot \theta_{i,s} \mid$ the absolute slopes of angles of incidence ($\theta_i \in [-\pi/2; 0]$) and of reflection ($\theta_s \in [-\pi/2; +\pi/2]$). S_1 denotes the monostatic statistical shadowing function (defined previously) inside the medium Ω_1, which is located above the rough surface Σ_A. Now if we substitute equation (3.1) in equation (3.5) then

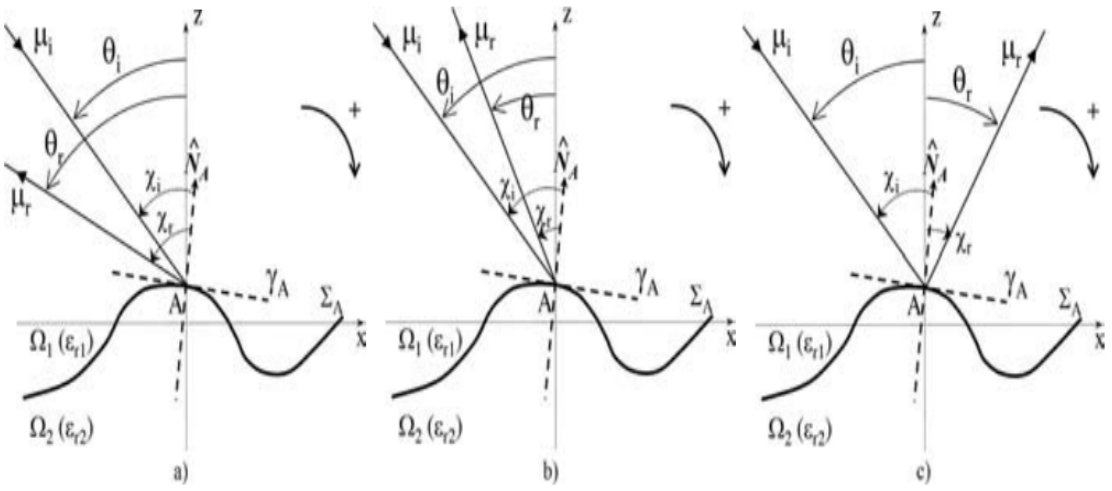

Figure 3.4: Configurations of the bistatic shadowing function in reflection: (a) $\theta_r \in [\pi/2; \theta_i[$, (b) $\theta_r \in [\theta_i; 0[$ and (c) $\theta_r \in [0; +\pi/2[$ [2]

we get:

$$S_{11}(\mathbf{K}_i, \mathbf{K}_r \mid \eta_A, \gamma_A) = \begin{cases} \Upsilon(\mu_r - \gamma_A)[\, P_h(\eta_A) - P_h(-\infty)]^{\,\Lambda(\mu_r)} & if \quad \theta_r \in [-\pi/2; \theta_i[\\ \Upsilon(\mu_i - \gamma_A)[\, P_h(\eta_A) - P_h(-\infty)]^{\,\Lambda(\mu_i)} & if \quad \theta_r \in [\theta_i; 0[\\ \Pi(\gamma_A)[\, P_h(\eta_A) - P_h(-\infty)]^{\,\Lambda(\mu_i)+\Lambda(\mu_r)} & if \quad \theta_r \in [0; +\pi/2[\end{cases} \tag{3.6}$$

where

$$\Pi(\gamma_A) = \begin{cases} 1 & if \quad \gamma_A \in [\,-\mu_i; +\mu_r] \\ 0 & otherwise \end{cases} \tag{3.7}$$

From equation (3.6), the restriction on the slope γ_A implies that $\gamma_A \in [\mu_r; +\infty]$, $\gamma_A \in [\mu_i; +\infty]$ and $\gamma_A \in [\mu_i; +\mu_r]$, respectively.

With MSP approximation [2], the bistatic shadowing function in reflection S_{11} is independent of the local tangent plane (or of the local surface slope), and then become as:

$$S_{11}(\mathbf{K}_i, \mathbf{K}_r \mid \eta_A, \gamma^{0(r)}) = \begin{cases} [P_h(\eta_A) - P_h(-\infty)]^{\Lambda(\mu_r)} & if \quad \theta_r \in [-\pi/2; \theta_i] \\ [P_h(\eta_A) - P_h(-\infty)]^{\Lambda(\mu_i)} & if \quad \theta_r \in [\theta_i; 0] \\ [P_h(\eta_A) - P_h(-\infty)]^{\Lambda(\mu_i)+\Lambda(\mu_r)} & if \quad \theta_r \in [0; +\pi/2] \end{cases} \tag{3.8}$$

Then, the only random variable inside the equation of the statistical shadowing function in reflection (3.8) is η_A, and then the avereging shadowing function which given from an arbitrary process becomes [29]:

$$S_{11}(\mathbf{K}_i, \mathbf{K}_r \mid \eta_A, \gamma^{0(r)}) = \begin{cases} 1/[1+\Lambda(\mu_r)] & if \quad \theta_r \in [-\pi/2; \theta_i] \\ 1/[1+\Lambda(\mu_i)] & if \quad \theta_r \in [\theta_i; 0] \\ 1/[1+\Lambda(\mu_i)+\Lambda(\mu_r)] & if \quad \theta_r \in [0; +\pi/2] \end{cases} \tag{3.9}$$

For a Gaussian process and Beckmann distribution [31], by substituting $\Lambda(\mu_{i,r})$ in equation (3.3).

Note that $\Lambda(\mu_a)$ can written as:

$$\Lambda(\mu_a) = \frac{erf(V_a) - 1}{2} + \frac{1}{2V_a\sqrt{\pi}} exp(-V_a^2) \tag{3.10}$$

where $erf(V_a) = 2/\sqrt{\pi} \int_0^{V_a} exp(-t^2)dt$, is the error function for each element of V_a, $V_a = \mu_a/\sigma_s\sqrt{2}$, $a \equiv \{i, r\}, \sigma_s$ is the surface root mean square (RMS) slope.

3.2 KA with Shadowing effect

After we introduced shadowing region effect and derive the equations of shadowing function S_{11}, shadowing correction factor is inserted to KA, and the results are checked with different incident angle θ_i and compared with MLFMM

.

Firstly, we demonstrate the shadowing function with incident angle $\theta_i = 80^o$ and observation angle $\theta_s \in [-\pi/2; +\pi/2]$ as shown in Figure 3.5.

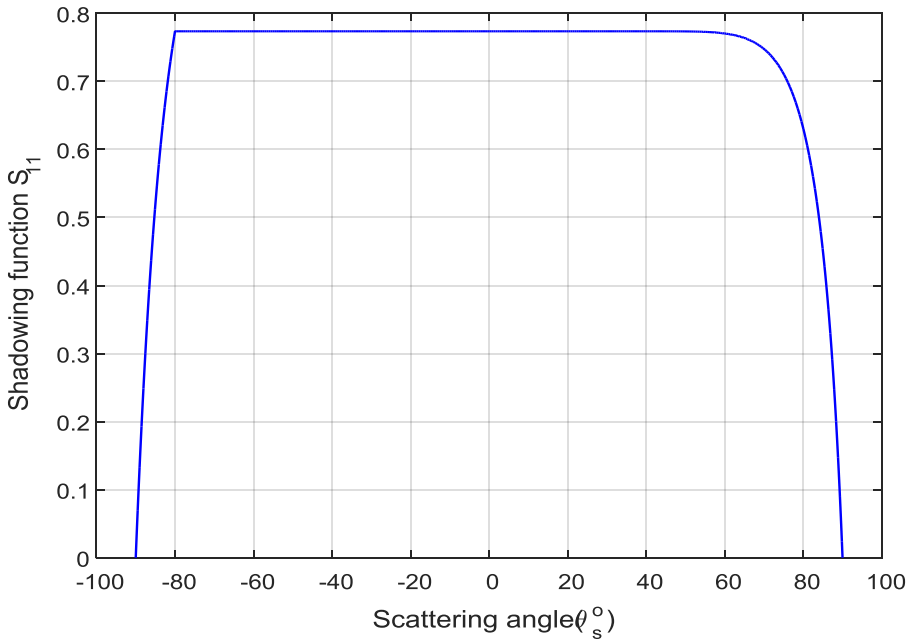

Figure 3.5: Bistatic shadowing function S_{11} with $\theta_i = -80^o$, $\theta_s \in [-\pi/2; +\pi/2], \sigma_s = 0.3$

The shadowing effect increases and become important as the incident angle θ_i increases over the range of scattering angle θ_s. Secondly the shadowing function will inserted to KA and equation (2.45) becomes:

$$\bar{\boldsymbol{\sigma}} = 4\pi R'^2 \begin{bmatrix} |S_{\theta\theta}|^2 & |S_{\theta\phi}|^2 \\ |S_{\phi\theta}|^2 & |S_{\phi\phi}|^2 \end{bmatrix} S_{11}. \tag{3.11}$$

Where S_{11} is the shadowing factor is given by equartion (3.9).

Consider a rough surface of dimension $10\lambda \times 10\lambda$ as shown in Figure 3.6, generated by Gaussian random process, of which autocorrelation function of height is given by $C_h(x, y) = \sigma_h^2 exp(-x^2/L_{cx}^2 - y^2/L_{cy}^2)$, the correlation lengths $L_{cx} = L_{cy} = 1.2\lambda_0$, and with standard deviation of the heights $\sigma_h = 0.2\lambda_0$, $(\sigma_s = \sqrt{2} \times \sigma_h/L_c \approx 0.24\lambda_0)$.

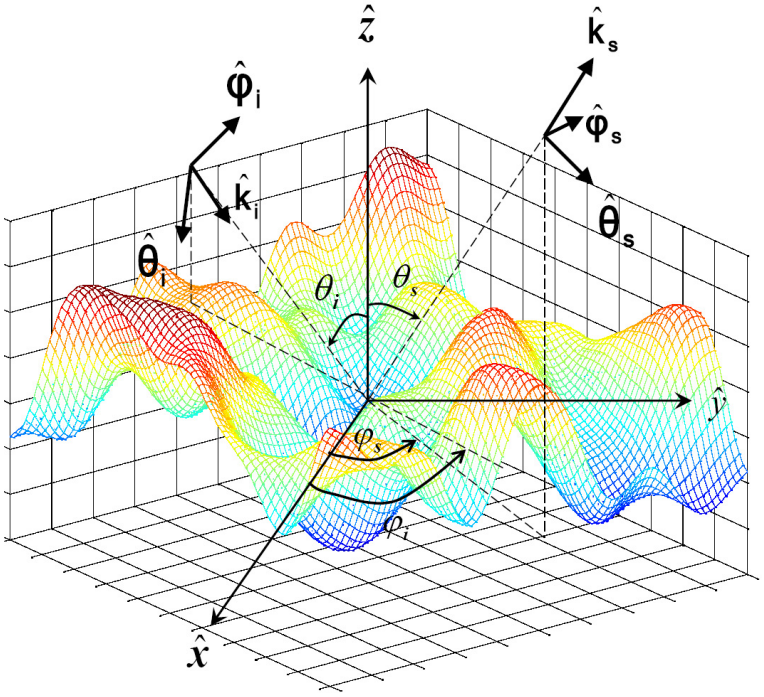

Figure 3.6: Geometry of the problem: illustration of the rough surface

The surface is illuminated by a plane wave in normal incident, $\theta_i = 0^o$, $\varphi_i = 0^o$, the scaling step of the surface are $\Delta_x = \Delta_y = \lambda_0/8$. The PO-with shadowing is compared to FEKO-PO as in Figure 3.7 , on which the RCS is plotted according to the angle of observation θ_s for both co-polarizations.

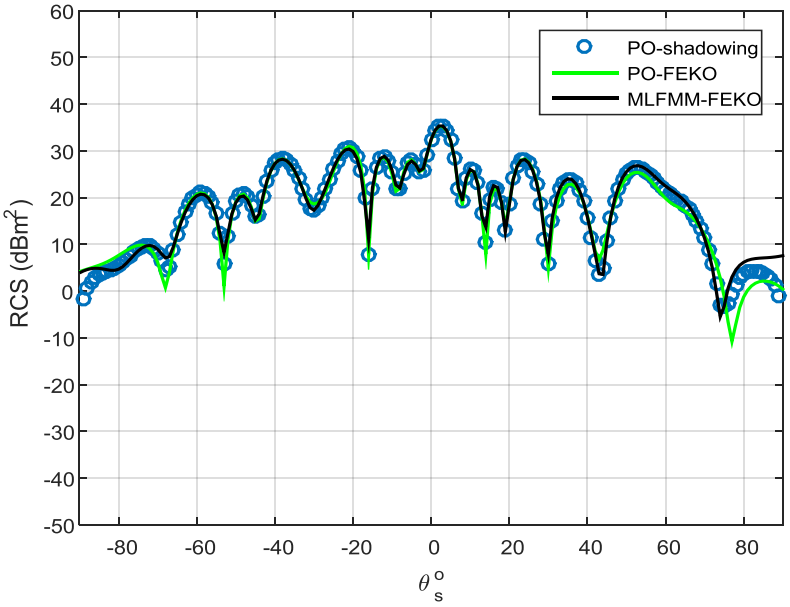

Figure 3.7: Comparison of bistatic RCS obtained with PO-with shadowing, FEKO-PO and PO proposed for HH co-polarization, case of a rough surface of dimension $10\lambda \times 10\lambda$, $\triangle x = \triangle y = \lambda_0/8$, $\theta_i = \phi_i = 0^o$, $L_{cx} = L_{cy} = 1.2, \sigma_s = 0.3, \sigma_h = 0.2\lambda$

We observe from Figure 3.7 that the result obtained by the proposed PO is nearly the same except at the edge and in good agreement with those get from FEKO. Now if we study the effect of shadowing by increase the incident angle $\theta_i = 60^o$.

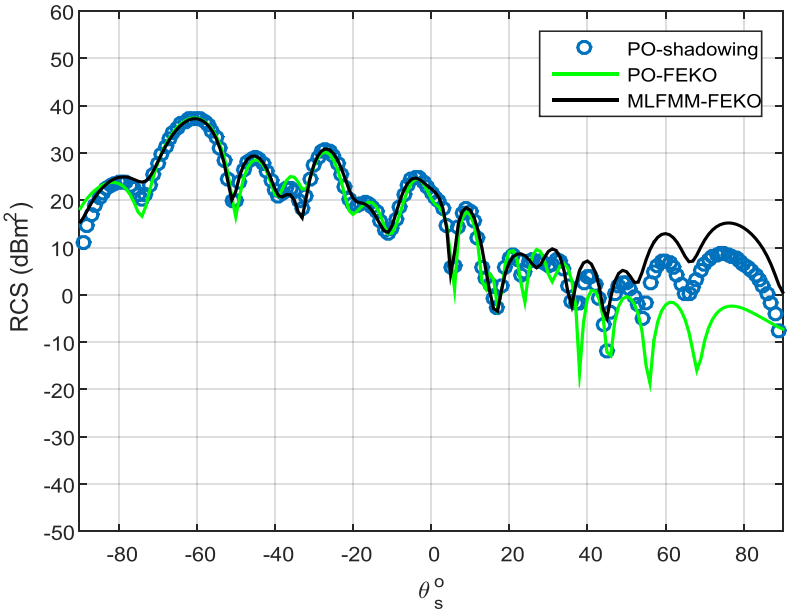

Figure 3.8: Comparison of bistatic RCS obtained with FEKO-PO and PO proposed for, case of a rough surface of dimention $10\lambda \times 10\lambda$, $\triangle x = \triangle y = \lambda_0/8$, $\theta_i = 80^o$, $L_{cx} = L_{cy} = 1.2, \sigma_s = 0.3, \sigma_h = 0.2\lambda$

As seen in Figure 3.8 we observe that KA approximation is effected more by shadowing phenomenon when θ_i increases, we observe that our proposed model still applicable and good compared with MOM. So this correction leads to improve the approximation at large scattering angles.

After we complete studying the shadowing effect and derive its formulation with KA and testing the validity of the proposed approximation, we will examine a new approximation in the last section which is called Iterative Physical Optics (IPO).

3.3 Iterative Physical Optics (IPO)

This section describes an application of the Iterative Physical Optics (IPO) method for computing the radio frequency (RF) scattering from electrically

large targets. The IPO method generates the electromagnetic current on the surface of the target, from which the scattered fields in the near-field and far-field regions can be computed. Much of the early development of the IPO method was focused on scattering by open-ended cavities [32], but it has also been applied to more general targets. The method of the iterative physical optics is much more efficient than purely numerical methods such as the MOM (or boundary integral method) and finite element method [18], because IPO is based on high frequency asymptotic principles of physical optics (PO) and uses a much coarser discretization density.

Generally, the scattering problem of rough surface is considered as an extra-large-scale electric scattering, for example 10,000 square lambda (λ, EM wavelength) [33]. It is more feasible to solve such a large-scale scattering problem using the analytical method rather than the numerical method. Many researchers focused on the KA, which is also called the PO [2].

According to the Huygens Principle, the volume induced current can be changed into the equivalent surface current. Those currents are the electric surface current $\mathbf{J}_s$ and the equivalent magnetic surface current $\mathbf{M}_s$ [7]. When the curvature radius R_c of the rough surface satisfies $R_c >> \lambda$, the rough surface can be regarded as many small planar patches put together, so the EM wave diffraction on the edge of the rough surface and the multiple scattering and multipath effect among the surface patches are ignored [33]. The induced currents ($\mathbf{J}_s$,$\mathbf{M}_s$) can be solved by the Fresnels equations under the computational costs . The IPO is based on a modified form of the magnetic field integral equation, as follows [35]:

$$\mathbf{J(r)} = \mathbf{J}^{(0)} + 2\hat{\mathbf{n}}(\mathbf{r}) \times \mathbf{H}_{IPO}(\mathbf{J}) \tag{3.12}$$

and

$$\mathbf{H}_{IPO}(\mathbf{J}) = P \int_{\boldsymbol{n.R'}<0} \mathbf{J(r')} \times \hat{\boldsymbol{R'}} \frac{e^{-ikR'}}{4\pi R'}(ik + \frac{1}{R'})dS' \tag{3.13}$$

in which $\mathbf{J(r)}$ is the surface current, $\hat{\mathbf{n}}$ is the surface normal unit vector, k is the wavenumber, and the integral is over the surface S' of the target. The symbol P indicates a principal value integral. Also, with $\boldsymbol{R'} = \mathbf{r} - \boldsymbol{r'}$ in which $\boldsymbol{r'}$ is the integration point on the surface (i.e., the source point) and $\mathbf{r}$ is the point at which the integral is evaluated (i.e., the test point), we have $\hat{\boldsymbol{R'}} = \boldsymbol{R'}/R'$ and $R' = |\boldsymbol{R'}|$. The lowest (zero) order IPO approximation $\mathbf{J}^{(0)}$ is appear as PO defined as follows:

$$\mathbf{J}^{(0)} = \begin{cases} 2\hat{\mathbf{n}}(\mathbf{r}) \times \mathbf{H}_i(\mathbf{r}) & for \quad \boldsymbol{\hat{n}.k} < 0 \\ 0 & for \quad \boldsymbol{\hat{n}.k} \geq 0 \end{cases} \tag{3.14}$$

Rather than being non-zero on only those parts of the surface that are geometrically illuminated by the incident field, this current is non-zero everywhere that the outward surface normal vector has a nonzero component in the direction opposite that of the incident plane wave.

These are directions for which the surface point would be illuminated by the incident plane wave in the absence of geometrical shadowing by other parts of the target surface. For non-convex surfaces, this is an important difference,

in that portions of the surface that are in the shadow of other parts of the target may have a non-zero lowest order IPO current.

A similar constraint, in the form of the condition $\hat{\mathbf{n}}.\boldsymbol{R'} < 0$, is also applied to the integral in (3.13), such that the integral may include portions of the surface that lie in the shadow of other parts of the target.

There are several methods for solving the IPO equations (3.13) and (3.14). The most straightforward approach is a simple iterative process [35].

$$\mathbf{J}^{(n)}(\mathbf{r}) = \mathbf{J}^{(0)}(\mathbf{r}) + 2\hat{\mathbf{n}}(\mathbf{r}) \times \mathbf{H}_{IPO}(\mathbf{J}^{(n-1)}) \tag{3.15}$$

where n is an iteration index. The interaction error ζ_s in the nth iteration step, is defined as follows [33]:

$$\zeta_s^{(n)} = \frac{|\mathbf{J}_s^{(n+1)} - \mathbf{J}_s^{(n)}|}{|\mathbf{J}_s^{(n)}|} \tag{3.16}$$

Once ζ_s is less than a residual error (e.g., 0.01), the interaction process is assumed to converge and reach a stable state.

3.4 Simulation Results of IPO

Since the IPO is derived from the magnetic field integral equation (MFIE), the interaction effects among all the patches of rough surface are taken into account, and they can improve the computational accuracy and extend the validity region of KA, compared with conventional PO. The Gaussian rough surface is used to quantize it.

The basic parameters are as follows: Size of rough surface $6\lambda \times 6\lambda$, correlation length of $L_c = 1.2\lambda$, root mean square height of rough surface is $\sigma_h = 0.2\lambda$. Set the incident angle as $\theta_i = 0^o$.

Obviously, it issatisfying the KA condition. The co-polarization including horizontal (HH) polarization and the vertical (VV) polarization are studied.

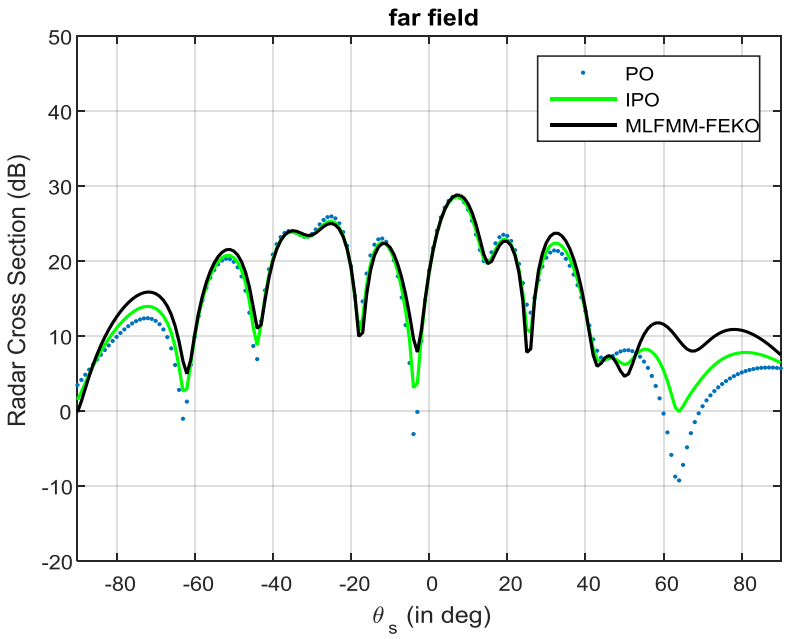

Figure 3.9: Comparison of bistatic RCS obtained with PO and IPO and FEKO-MLFMM for HH co-polarization, case of a rough surface of dimension $6\lambda \times 6\lambda$, $\triangle x = \triangle y = \lambda_0/8$, $\theta_i = \phi_i = 0^o$, $L_{cx} = L_{cy} = 1.2, \sigma_h = 0.2\lambda$

Radar cross section (σ) is calculated using the PO, IPO, and the rigorous MLFMM (which is considered as the reference data in this work). And the validity of IPO compared with MLFMM and PO, illustrated Figure 3.9.

IPO shows a good agreement with the rigorous method, even though the surface is rough .

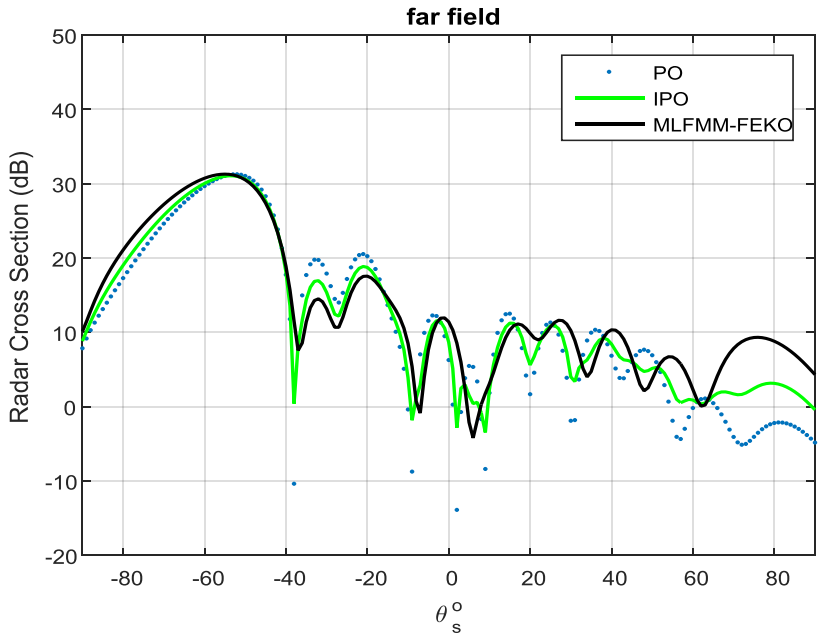

Figure 3.10: Comparison of bistatic RCS obtained with PO and IPO and FEKO-MLFMM, case of a rough surface of dimension $6\lambda \times 6\lambda$, $\triangle x = \triangle y = \lambda_0/8$, $\theta_i = 60^o$, $L_{cx} = L_{cy} = 1.2, \sigma_h = 0.2\lambda$

At the large incident angle ($\theta_i = 60^o$), as shown in Figure 3.10 Radar Cross Section scattering coefficient (σ) is given out using the PO, IPO, and the rigorous MLFMM.

The validity of IPO compared with MLFMM is illustrated in Figure 3.10 IPO shows a good agreement with the rigorous method , even though the surface is rough and the incident angle is large.

To conclude, previous approximations (PO, PO-shadowing and IPO) are called asymptotic models and useful to be applied when the surface is large due to their simplifying assumptions, less complexity and low computational time and capacity, but these techniques are restricted by their validity domain.

Conclusion

In this thesis we studied the scattering of an electromagnetic wave by a 2D random rough surface (3D electromagnetic problem) using asymptotic models. Since remote sensing technology becomes very important in different field especially in telecommunication and military, so many techniques appear and are developed to calculate Radar Cross Section (RCS) such as the Method of Moments (MOM) and it's accelerations, but these methods are too complex and need high computational time and capacity, and applicable for small surface dimensions less than $30\lambda \times 30\lambda$.

In this work we adopted an asymptotic technique called Kirchhoff Approximation (KA) which is a simple approximation need less computational time and capacity, applicable for large rough surfaces more than $100\lambda \times 100\lambda$. then a mathematical model based on KA is studied and the validity of the proposed model is checked by comparing the results of the RCS with the accelerated rigorous method called Multi Level Fast Multipole Method (MLFMM).

According to the results of the Radar Cross Section (RCS) of rough surface, we observed that this model provides a good agreements with rigorous method except at the edge due to facts that KA did not take into account the concentration of currents at the edge and the shadowing phenomenon, so to overcome this problem, and to improve the model a correction factor called bistatic shadowing function is inserted to the KA math model. As a result, the KA model with the shadowing function becomes more accurate, but not exact as a rigorous method.

Finally, in order to improve the results especially at the boundaries, an iterative approach called Iterative Physical Optics (IPO) based on the Magnetic Field Integral Equation (MFIE) used. The method uses simple and efficient approaches for the computation of surface current interactions. Numerical results of scattering fields show that the proposed approach is preferable in EM problems where the diffraction effects or currents in shadow regions would cause large errors.

As future work, we can apply the previous study for the case of two scatteres (object above rough surface). A Hybrid technique of IPO and KA can be developed to calculate the scattered field from the total scene. The interaction between the object and the rough surface can be calculated iteratively while the KA can be applied only on the rough surface.

Glossary and Abbreviation

EFIE Electric Field Integral Equation

FDTD Finite Difference Time-Domain

FSA Forward Scattering Alignment

GO Geometric Optics

IPO Iterative Physical Optics

KA Kirchhoff Approximation

LHI Liner Homogenous Isotropic

MoM Method of Moment

MSP Method of Stationary Phase

PDF Power Distribution Function

PO Physical Optics

PC Perfect Conductor

PPW Plane Progressive Wave

RCS Radar Cross Section

RMS Root Mean Squar

SPM Small Perturbation Method

SSA Small Slop Approximation

$\boldsymbol{S_{11}}$ Shadowing Function

TE polarization Transverse Electric (polarizationn H)

TM polarization Transverse Magnetic (polarization V)

$\boldsymbol{Z_0}$ Intrinsic impedance

$\boldsymbol{\epsilon}_0$ Permittivity of free space

$\boldsymbol{\mu}_0$ Permeability of free space

$\boldsymbol{\eta}$ RMS surface height

$\boldsymbol{\theta}_i$ Incident angle

$\boldsymbol{\theta}_s$ Scattered Angle

Bibliography

[1] E.H Newman and K. Kingsley, "An introduction to method of moments", Jornal of Computer Physics Communications, Vol. 68, pp. 1-18, August, 1990.

[2] N. Pinel and C Bourlier, Electromagnetic Wave Scattering from Random Rough Surfaces (Asymptotic Models), First published 2013 in Great Britain and the United States by ISTE Ltd and John Wiley & Sons, Inc.

[3] W. Gordan, "Far-Field Approximation to the Kirchhoff-Helmholtz Representation of Scattered Fields", IEEE Transactions on Antennas and Propagation, Vol. 68, pp. 590-592, July 1975.

[4] C. Corbel, C. Bourlier, N. Pinel and J. Chauveau, "Rough surface RCS measurements and simulations using the Physical Optics Approximation", IEEE Transactions on Antennas and Propagation, Institute of Electrical and Electronics Engineers, pp. 5155-5165, December 2013.

[5] J. Wiley, Standard Test Procedures for Antennas, ANS/IEEE Std.149-1979, New York, 1979.

[6] J. A. Kong, Electromagnatic wave theory, EMW Publishing,Cambridge, USA, 2008.

[7] M. Kouali, "Diffusion d'une onde electromagentique par un objet audessus d'une surface rugueuse Probleme vectoriel 3D", PhD dissertation, Universite de Nantes, Septembre 2012

[8] J. Song, C. Lu and W. Chew, "Multilevel fast multipole algorithm for electromagnetic scattering by large complex object", IEEE Transactions on Antennas and Propagation, Vol. 45, pp. 1488-1493.

[9] W. Chew, J. Jin, C. LU, E.Michielssen and J. Song, "Fast solution methods in electromagnetic", IEEE Transactions on Antennas and Propagation, vol. 45, pp. 533-543, March 1997.

[10] M.Saillard, A.Sentenac "Rigorous solutions for electromagnetic scattering from rough surfaces", Waves in Random Media, vol. 11, , pp. 103137, July 2001.

[11] K. Warnick and W. Chew, "Numerical simulation methods for rough surface scattering", Jornal of Waves in Random Media, Vol. 11, pp. R1-R30, 2001.

[12] N. Abd Rashid, K. Othman and N. Ahmad, "Analysis on Radar Cross Section of Different Target Specifications for Forward scatter Radar (FSR)", IEEE fourth International Conference on Digital Information and Communication Technology and its Applications (DICTAP), May 2014

[13] L. Tasang, J. Kong, and R. Shin, Theory of Microwave Remote Sensing, Wiley Series in Remote Sensing and Image Processing, 1985.

[14] M. Mansuripur, Clasical Optics and its Applications, First published 2002 in Cambridge University Press.

[15] N. de Beaucoudrey, P. Schott,C. Bourlier, "Detection of oil slicks on sea surface depending on layer thickness and sensor frequency", IEEE International Geoscience and Remote Sensing Symposium, Toulouse, France, pp. 2741-2743, July 2003

[16] W. Peake, "Theory of radar return from terrain", IRE National Convention Record, Vol. 1, pp. 27-41, March 1959.

[17] J. Johnson, "Third-order small-perturbation method for scattering from dielectric rough surfaces", Journal of the Optical Society of America, Vol. 16, pp. 2720-2736, November 1999.

[18] B. Stupfel, "A hybrid finite element and integral equation domain decomposition method for the solution of the 3-D scattering problem", Journal of Computational Physics, Vol. 172, pp. 451-471, September 2001.

[19] M. Ribeiro, Gaussian Probability Density Functions: Properties and Error Characterization. Institute for system and Robotics, Instituto Superior Tcnico, February 2004.

[20] E. Thorsos, "The validity of the Kirchhoff approximation for rough surface scattering using a Gaussian roughness spectrum ", Journal of the Acoustical Society of America, Vol. 83, pp. 78-92, January 1988

[21] L. Rayleigh, J.Willliam, M. A and F. RS , The Theory of Sound, Vol. 1, New York, 1945.

[22] E. Knotl, J. Schaeffer and M.Tulley, Radar Cross Section , Scitech Publishing, Second Edition, 2004.

[23] G. Kubicke, Y. Yahia, C. Bourlier, N. Pinel, and P. Pouliguen, "Bridging the gap between the babinet principle and the physical optics approximation : Scalar problem", IEEE Transactions on Antennas and Propagation, Vol. 59, pp. 4725-4732, 2011.

[24] L. Boithias, Radio Wave Propagation, North Oxford Academic Publishers, London, 1987.

[25] F. Shi, W. Choi, M. Lowe1, E. Skelton and R. V. Craster, "The validity of Kirchhoff theory for scattering of elastic waves from rough surfaces", April 2015.

[26] J. West, "Investigation of shadowing in rough surface scattering at small grazing agnle", Proceeding of IEEE Antenna and Propagation Society International Symposium and URSI National Radio Science Meeting, Vol. 3, June 1994.

[27] R. J. Wagner, "Shadowing of Randomly Rough Surfaces", Journal of the Acoustical Society of America, Vol.41, July 2005.

[28] B. Smith, "Geometrical shadowing of a random rough surface", IEEE Transactions on Antennas and Propagation, Vol. 15, pp. 668-671, September 1967.

[29] C. Bourlier, C. Berginc and J. Saillard, "Bistatic scattering coefficient from one- and two dimensional random surfaces using the stationary phase and scalar approximation with shadowing effect-comparisons with experiments and application to the sea surface ", Journal of Waves in Random Media, Vol. 11, pp.119-147, August 2006.

[30] C. Bourlier, C. Berginc and J. Saillard, "Monostatic and bistatic statistical shadowing functions from a one-dimensional stationary randomly rough surface: II. Multiple scattering",Journal of Wave in Random Media, Vol. 12, pp.175-200, August 2006.

[31] E. Hetz, "Understanding the masking-shadowing function in Microfacet-Based BRDFs", Journal of Computer Graphics techniques, Vol. 3, pp. 48-107, 2014.

[32] F. Obelleiro-Basteiro, J. Rodriguez and R. Burkholder, "An iterative physical optics approach for analyzing the electromagnetic scattering by large open-ended cavities", Transactions on Antennas and Propagation, Vol. 43, pp. 356-361, April 1993.

[33] C. Li, C. Tong, L. Qi, T. Wang and D. Sui, "An Accelerated Forward-Backward Iterative Physical Optics for Electromagnetic Scattering from Rough Sea Surface", Taylor andFfrancis Journal of Electromagnetics Electromagnetics, Vol. 35, pp.26-537, 2015.

[34] W. Yang, Z. Zhao, C. Qi, W. Liu, and Z. P. Nie, "Iterative hybrid method for electromagnetic scattering from a 3-D object above a 2-D random dielectric rough surface", Journal of Progress in Electromagnatics Research (PIER), Vol. 117. pp. 435-448, 2011.

[35] Y. Kwan and G. Bohannon, "Electromagnetic Scattering Calculations by Iterative Physical Optics for Engineering Applications", IEEE Radar Conference (RadarConf), June 2017.

نماذج وتقنيات تقريبيه لدراسة ظاهرة انعكاس الموجات الكهرومغناطيسي (EM) عن سطوح غير منتظمه هندسيا ثنائية الابعاد (2D) .

إعداد : اشرف طلال أحمد ربايعه

المشرف : د. محمد كوعلي

ملخص :

يعتبر البحث والدراسة في مجال انعكاس الأشعة من السطوح الغير منتظمة هندسيا والعشوائية أمرا هاما للعديد من المجالات العلمية والهندسية مثل , توليد الصور الواقعية في الرسومات الحاسوبية , وتصنيع أشباه الموصلات , وفحص تباين السطوح في الالكترونيات الدقيقة, كل هذه الأمور وغيرها, أبرزة أهميه دراسة انعكاس الأشعة عن سطوح غير منتظمة هندسيا. في الوقت الحاضر, يستمر البحث والدراسة في هذا المجال, بسبب ظهور وتطور العديد من المجالات والتطبيقات التي تعنى بالسطوح العشوائية والغير منتظمة وليس لها توزيع منتظم, مثل الاتصالات السلكية واللاسلكية وتطبيقات الأشعة السينية في الصور الطبية والقطاع العسكري وتطبيقات الاستشعار عن بعد. لهده الأسباب وغيرها تم تطوير عدة أنظمه وتقنيات مثل(MOM), لدراسة وحساب المقطع الراداري (RCS) حيث من خلال معرفته وحسابه نستطيع معرفة ماهية وطبيعة السطوح الصادرة عنها الموجات الكهرومغناطيسية والإشارات دون الحاجة إلى الاتصال المباشر بالسطوح واخذ عينات منها لفحصها ومعالجتها وبالتالي معرفه ماهية وطبيعة هذه السطوح, ولكن مشكله هذه التقنيات والدوال أنها معقده وبحاجه إلى إمكانيات وقدرات عاليه في الأجهزة الحوسبة والالكترونيات وبالتالي وقت وجهد وتكاليف عاليه.

وبدلا من هذه التقنيات المعقدة والمكلفة , ابتدأ البحث عن أساليب وتقنيات جديد اقل تكلفه ووقت حتى لو كانت تقريبية واقل دقه, ونتيجة لهذه الأسباب وغيرها قمنا بدراسة وتطبيق تقنيه لحساب المقطع الراداري (RCS), تعرف باسم داله كيرشوف (KA) , أو البصريات الفيزيائية (PO) في حالة السطوح ثلاثية الأبعاد (3D) بحيث تكون أسرع واقل تكلفه, وتحتاج القليل من الوقت الحسابي. في حين أن التقنيات المعقدة والدقيقة (MOM) تسمح بمعالجه وحساب RCS للأسطح ذات الإبعاد المحدودة بحيث تكون اقل من (30λ×30λ) للأسطح ثلاثية الإبعاد (3D) , في حين إن الدالات التقريبية

مثل تلك التي قمنا بتطبيقها وتبنيها (KA) للأسطح ثلاثيه الإبعاد (3D) تتيح لمعالجه وحساب RCS للأسطح ذي الإبعاد الكبيرة أكثر من ($100\lambda \times 100\lambda$) ولكن ضمن محددات و نطاق انطباق هذه الدوال في العادة يكون حساس وصارم في التطبيق.

إن الهدف الرئيسي من هذه الأطروحة هو عمل دراسة ومقارنة لداله رياضيه (KA) والتي تعنى بحساب المقطع الراداري من خلال حساب الموجات الكهرومغناطيسية المرتدة والمنعكسة من سطوح ثلاثية الإبعاد (3D) الخشنة والغير منتظمة هندسيا, ومن ثم مقارنتها بتقنيات دقيقه مثل الدالة المسرعة من (MOM) وهي (MLFMM), للتأكد من صحتها ومدى دقتها في حساب المقطع الراداري (RCS). ولتحسين فاعليتها ودقتها قمنا باضافة دراسة لمعامل تصحيح يعتمد على ظاهرة الظل نتيجة خشونة السطوح وزاوية السقوط يسمى معامل الظل. بحيث قمنا بدراسة معادلاته وتطبيقها في دالة (KA) وفحص مدى الدقة التي يضيفا في عمليات الحساب. تتم المقارنة بين التقنيات على كامل نطاق زاوية الانعكاس من الجسم العشوائي ($[-90^\circ : +90^\circ]$) .

لقد تم تنظيم الأطروحة على النحو التالي: أولا، تقديم بعض المفاهيم والمبادئ الأساسية في النظرية الكهرومغناطيسية اللازمة, مثل التمثيل الإحصائي لوصف الأسطح العشوائية بحيث يمكن دراستها ووصفها، دراسة انعكاس الأشعة من السطوح الخشنة ، والمعادلة التكاملية القائمة على مبدأ Huygens وما إلى ذلك.

أما في الفصل الثاني، سوف يتم تقديم دراسة لنموذج رياضي (KA) لحساب المقطع الراداري (RCS) للسطوح الخشنة العشوائية ثلاثية الأبعاد (3D), مع توضيح خصائصه ومدى صلاحيته ومدى فاعليته في حساب المقطع الراداري. في الواقع، يتم التأكد من فعاليته بمقارنته مع التقنيات الدقيقة للتأكد من دقته وإمكانية تطبيقه. لتحسين التقنية ومراعاة المنطقة المتأثرة بظاهرة التظليل قمنا بتطبيق معادلات عامل الظل لزيادة فاعلية ودقة النمودج, وفي النهاية سوف يتم مناقشة نموذج جديد يعرف بتقنية تكرار البصريات الفيزيائية (IPO) الذي يعتمد بحساباته على النموذج المقدم (KA) ولكن بطريقه تكراريه توضح علاقة التيار بين أجزاء السطح.